

Copyright  
by  
Matthew C. Dykstra  
2015

The Thesis committee for Matthew C. Dykstra  
Certifies that this is the approved version of the following thesis:

**Single Station Doppler Tracking for Satellite Orbit Prediction  
and Propagation**

APPROVED BY

SUPERVISING COMMITTEE:

---

Wallace T. Fowler, Supervisor

---

E. Glenn Lightsey

**Single Station Doppler Tracking for Satellite Orbit Prediction  
and Propagation**

**by**

**Matthew C. Dykstra, B.S.E.E.**

**THESIS**

Presented to the Faculty of the Graduate School of  
The University of Texas at Austin  
in Partial Fulfillment  
of the Requirements  
for the Degree of

**MASTER OF SCIENCE IN ENGINEERING**

THE UNIVERSITY OF TEXAS AT AUSTIN

May 2015

To Melissa, for always supporting me as I move all across the country, and my  
parents, without whom I would never have made it this far.

# **Single Station Doppler Tracking for Satellite Orbit Prediction and Propagation**

Matthew C. Dykstra, M.S.E.  
The University of Texas at Austin, 2015

Supervisor: Wallace T. Fowler

Presently, there are two main methods of launching a cube satellite into Earth orbit. The first method is to purchase a secondary payload slot on a major launch vehicle. For the second method, the satellite must first be transported via a major launch vehicle to the International Space Station. From there, the satellite is loaded into one of two deployment mechanisms, and deployed at a specified time. In each case, the satellite's initial orbit is not accurately known. For ground operators this poses a problem of position uncertainty. In order to solve this problem, a satellite tracking algorithm was developed to use an initial two-line element set for coarse orbit prediction, followed by Doppler measurements for continuous processing and updating. The system was tested using simulated data. The analysis showed that this low-cost, scalable system will satisfy the tracking requirements of many cube satellite missions, including current missions at the University of Texas.

# Table of Contents

|  |           |
|--|-----------|
| <b>Abstract</b>  | <b>v</b>  |
| <b>List of Figures</b>   | <b>ix</b> |
| <b>Chapter 1. Introduction</b>                                   | <b>1</b>  |
| 1.1 Doppler Shift . . . . .                                      | 2         |
| 1.2 Cube Satellite Standard . . . . .                            | 4         |
| 1.3 Background . . . . .   | 6         |
| 1.4 Contributions . . . . .                                      | 7         |
| 1.5 Thesis Organization . . . . .                                | 8         |
| <b>Chapter 2. Motivation</b>                                     | <b>9</b>  |
| 2.1 Primary Motivations . . . . .                                | 10        |
| 2.2 Secondary Motivations . . . . .                              | 11        |
| <b>Chapter 3. Technical Components</b>                           | <b>13</b> |
| 3.1 Reference Frames . . . . .                                   | 13        |
| 3.1.1 Orbital Elements . . . . .                                 | 14        |
| 3.1.2 Earth-Centered Inertial Frame (ECI) . . . . .              | 15        |
| 3.1.3 Earth-Centered Earth-Fixed Frame (ECEF) . . . . .          | 16        |
| 3.1.4 Topocentric Frames . . . . .                               | 18        |
| 3.1.5 Geocentric & Geodetic Coordinates . . . . .                | 19        |
| 3.2 Conversions . . . . .  | 20        |
| 3.2.1 Conversion of a State Vector to Orbital Elements . . . . . | 21        |
| 3.2.2 Conversion of Orbital Elements to a State Vector . . . . . | 23        |
| 3.2.3 Conversion From ECI to ECEF . . . . .                      | 25        |
| 3.2.4 Conversion Between ECEF and Topocentric Frames . . . . .   | 26        |
| 3.2.5 Conversion from ECEF to LLH . . . . .                      | 27        |
| 3.3 Dynamical Models & Numerical Integration . . . . .           | 29        |

|                   |   |           |
|-------------------|---|-----------|
| 3.3.1             | J2 Perturbation Model & Integration . . . . .         | 29        |
| 3.3.2             | Drag Model & Integration . . . . .                    | 31        |
| 3.4               | Time Systems . . . . .                                | 33        |
| 3.4.1             | Julian Date & Modified Julian Date . . . . .          | 33        |
| 3.4.2             | Unix Time . . . . .                                   | 34        |
| <b>Chapter 4.</b> | <b>Ground Station Construction and Operations</b>     | <b>35</b> |
| 4.1               | Hardware . . . . .                                    | 35        |
| 4.1.1             | Computers & Software-Defined Radios . . . . .         | 36        |
| 4.1.2             | Amplifiers . . . . .                                  | 36        |
| 4.1.3             | Antennas . . . . .                                    | 37        |
| 4.1.4             | Cabling . . . . .                                     | 39        |
| 4.2               | System Configurations . . . . .                       | 39        |
| 4.2.1             | Ground Transmission System . . . . .                  | 39        |
| 4.2.2             | Ground Receiving System . . . . .                     | 40        |
| 4.3               | Doppler Tracking Hardware Advantage . . . . .         | 41        |
| 4.4               | Ground Station Assumptions . . . . .                  | 43        |
| 4.5               | Station Scheduling . . . . .                          | 44        |
| 4.5.1             | Pass Strength Considerations . . . . .                | 44        |
| 4.5.2             | Management of Position Uncertainty . . . . .          | 46        |
| 4.5.3             | Management of Onboard Memory . . . . .                | 47        |
| 4.5.4             | High Priority Communications . . . . .                | 48        |
| <b>Chapter 5.</b> | <b>Orbit Prediction and Tracking Algorithms</b>       | <b>49</b> |
| 5.1               | Mode 1: Initial Orbit Prediction & Modeling . . . . . | 49        |
| 5.1.1             | Mode 1 Goal . . . . .                                 | 50        |
| 5.1.2             | Procedures . . . . .                                  | 51        |
| 5.1.3             | Resulting Outputs . . . . .                           | 53        |
| 5.1.4             | Two-Line Element Sets . . . . .                       | 55        |
| 5.2               | Mode 2: Continuous Orbit Model Update . . . . .       | 56        |
| 5.2.1             | Mode 2 Goal . . . . .                                 | 57        |
| 5.2.2             | Procedures . . . . .                                  | 58        |
| 5.2.3             | Resulting Outputs . . . . .                           | 59        |
| 5.2.4             | Slant-Range Rate Derivation . . . . .                 | 60        |

|                     |  |           |
|---------------------|--|-----------|
| 5.2.5               | General Batch Estimation Algorithm . . . . .               | 61        |
| 5.2.6               | Slant-Range Rate Batch Estimation Implementation . . . . . | 64        |
| <b>Chapter 6.</b>   | <b>Prediction Fidelity Analysis</b>                        | <b>67</b> |
| 6.1                 | Pass Frequency Investigation . . . . .                     | 67        |
| 6.1.1               | Inclination-Based . . . . .                                | 68        |
| 6.1.2               | Pass Strength Inclusion . . . . .                          | 69        |
| 6.2                 | Prediction Error Sources and Rates . . . . .               | 74        |
| 6.2.1               | Dynamical Model Errors . . . . .                           | 74        |
| 6.2.2               | Integrator Error . . . . .                                 | 75        |
| 6.3                 | Expanded Network Potential . . . . .                       | 76        |
| <b>Chapter 7.</b>   | <b>Tracking Analysis and Results</b>                       | <b>78</b> |
| 7.1                 | Mode 1 Testing and Results . . . . .                       | 78        |
| 7.1.1               | Test Case Selection . . . . .                              | 78        |
| 7.1.2               | Orbit Prediction Results . . . . .                         | 79        |
| 7.2                 | Pass Selection and Observation . . . . .                   | 82        |
| 7.2.1               | Manual Pass Selection . . . . .                            | 82        |
| 7.2.2               | Simulated Observation Data . . . . .                       | 82        |
| 7.3                 | Mode 2 Testing and Results . . . . .                       | 84        |
| 7.3.1               | Time Matching . . . . .                                    | 85        |
| 7.3.2               | Initial Nominal State Selection . . . . .                  | 85        |
| 7.3.3               | Orbit Prediction Results . . . . .                         | 86        |
| <b>Chapter 8.</b>   | <b>Conclusions and Future Work</b>                         | <b>90</b> |
| 8.1                 | Conclusions . . . . .                                      | 90        |
| 8.2                 | Future Work . . . . .                                      | 91        |
| <b>Bibliography</b> |  | <b>93</b> |



## List of Figures

|     |  |    |
|-----|--|----|
| 1.1 | Graphical representation of the Doppler shift from an object moving to the left[5]. . . . .  | 3  |
| 1.2 | The Doppler curve produced from ground station observations of a passing LEO satellite. . . . .  | 4  |
| 1.3 | Cube satellite payload fairing and deployment structure called the P-POD[7]. . . . .   | 5  |
| 1.4 | RACE satellite, created by the Texas Spacecraft Laboratory. . . . .  | 6  |
| 3.1 | Graphical representation of the orbital elements for a typical orbit[13].  | 15 |
| 3.2 | Graphical representation of true anomaly compared to eccentric anomaly for an orbiting satellite[18]. . . . .  | 16 |
| 3.3 | Satellite orbit viewed in the ECI frame. Axes are aligned with the celestial sphere and do not rotate with the Earth. . . . .  | 17 |
| 3.4 | Satellite orbit viewed in the ECEF frame. Axes rotate with the Earth allowing major movements relative to the Earth's surface to be seen.  | 17 |
| 3.5 | Antenna pointing with associated direction angles aligned in the ENU frame[23]. . . . .  | 19 |
| 3.6 | Graphical representation of the difference between geocentric latitude and geodetic latitude[8]. . . . .   | 20 |
| 3.7 | Orbital elements and the instantaneous corresponding state vector. .   | 25 |
| 4.1 | Mounted Antennas used by the Texas Spacecraft Laboratory. . . . .  | 38 |
| 4.2 | System Diagram for the transmitting portion of the ground station. .   | 40 |
| 4.3 | System Diagram for the receiving portion of the ground station. . .  | 41 |
| 4.4 | Elevation curve displaying a low-elevation pass. This satellite pass peaks at a low elevation which means that the slant range is long and the satellite is overhead for a shorter period of time. This is an example of a lower quality pass. . . . . | 45 |
| 4.5 | Elevation curve displaying a high-elevation pass. This pass peaks at a higher elevation meaning that it is more directly overhead and the slant range is smaller. This is an example of a higher quality pass.   | 46 |
| 5.1 | Satellite track passing above the 80° limit. . . . .   | 55 |

|      |  |    |
|------|--|----|
| 5.2  | A modified satellite track created to ensure the rotors keep pace with the satellite's motion. . . . .   | 55 |
| 5.3  | Two-Line Element Set[21]. . . . .  | 56 |
| 6.1  | “Shark-fin” style graph showing total passes over a 30 day span. . .   | 69 |
| 6.2  | Time between each satellite pass over a 30 day span. . . . .   | 70 |
| 6.3  | Total satellite passes reaching above 30° elevation over a 30 day span.  | 70 |
| 6.4  | Time between each pass above 30° elevation during a 30 day span. .   | 71 |
| 6.5  | Total satellite passes reaching above 50° elevation over a 30 day span.  | 72 |
| 6.6  | Time between each pass above 50° elevation during a 30 day span. .   | 72 |
| 6.7  | Total satellite passes reaching above 70° elevation over a 30 day span.  | 73 |
| 6.8  | Time between each pass above 70° elevation during a 30 day span. .   | 73 |
| 6.9  | Graph depicting position differences over time for different models. Gravity models are compared to the next most significant[1]. . . . .  | 75 |
| 7.1  | Initial propagation parameters reported by the mode one program execution in Matlab. These parameters correspond specifically to the ISS. . . . .  | 79 |
| 7.2  | Ground track of the resulting 24-hour propagation displays the two-dimensional trajectory of the spacecraft overlaying the Earth. . . . .  | 80 |
| 7.3  | Three-dimensional plots of the spacecraft's trajectory seen in two different frames. . . . .   | 80 |
| 7.4  | Skyplot displaying each of the six overhead predicted passes. . . . .  | 81 |
| 7.5  | Plot of the elevation versus time for the pass selected for processing.  | 83 |
| 7.6  | Sky plot of the pass selected for processing. . . . .  | 83 |
| 7.7  | A portion of the true Doppler shift curve and simulated observations with added Gaussian noise. . . . .  | 84 |
| 7.8  | Ground track of the resulting 24-hour propagation from the starting time of pass used in mode two displays the two-dimensional trajectory of the spacecraft overlaying the Earth. This track overlaps the original from mode one for the time following the observed pass, but also continues forward until the new 24-hour propagation is complete. . . . . | 86 |
| 7.9  | Three-dimensional plots of the spacecraft's trajectory seen in two different frames. . . . .   | 87 |
| 7.10 | Skyplot displaying each of the seven overhead predicted passes. . .  | 88 |
| 7.11 | Elevation plots for the initial and the final trajectories for the processed pass. . . . .   | 88 |

# Chapter 1

## Introduction

Cube satellite projects are now a widespread method of sending small-scale payloads to space in order to do scientific research, technology demonstrations, and various other missions. The cube satellite concept provides many people in both academia and private industry with the ability to see their projects transformed from idea to reality[6]. Sending smaller payloads into space has numerous advantages ranging from cost to development time, but it is not without some challenges. Using smaller, standardized structures casts limitations on the overall size, weight, and power of the hardware involved. This often forces engineers to push certain areas of the design at the cost of others.

In specific circumstances, designers may choose not to equip their satellite with a space-qualified GPS receiver. This decision could be made due to limits on communication bit rates, power budgets, size limitations, or other constraints. In other cases mission designers may overlook a high fidelity navigation instrument simply because such accurate knowledge of position is not necessary in order to satisfy the mission requirements. In the case of the Radiometric Atmospheric CubeSat Experiment (RACE) mission at the University of Texas, a flight GPS receiver was left out in place of other attitude and scientific hardware[28]. Whatever the case may be, a reasonable knowledge of the satellite's orbit characteristics and position

over time is required for scheduling and mission operations. In order to uplink commands, receive downlinked science data or telemetry, or diagnose a problem during flight, operators must know where the satellite is in order to direct high gain antennas from ground stations to communicate.

The challenges of orbit determination and track maintenance from a single ground station in the absence of GPS are explored in this thesis. Additionally, the ground operations relating to these tasks is introduced and discussed.

## **1.1 Doppler Shift**

The Doppler shift is a phenomenon in which the frequency of a wave changes, up or down, as experienced by an observer moving relative to the source of the wave. The most common example of this frequency shift is found when listening to a car as it moves past an observer. As the car passes the observer, the sound shifts to a noticeably lower pitch. When the car is moving towards the observer, the sound waves are seemingly compressed, causing an upward shift in the pitch. This is because each successive wave is emitted at a closer position to the observer, causing it to take a slightly lesser amount of time to reach the observer. As the car is moving away, each wave is emitted from slightly farther away than the previous. This makes the sound waves seemingly spread apart and lowers the pitch of the noise.

The Doppler phenomenon has applications throughout many different scientific fields, from astronomy to medical imaging, but one in particular applies to satellite orbit determination. If an observer is placed at a point on the surface of the

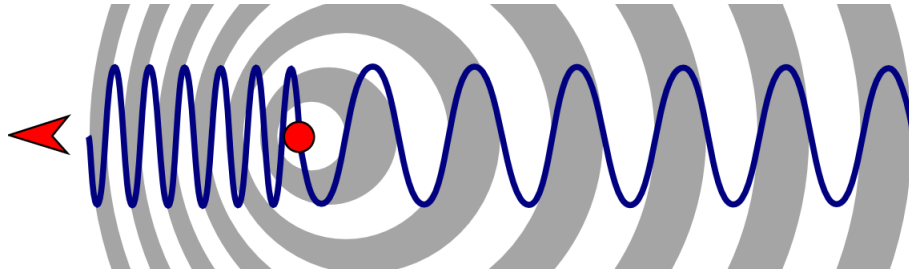


Figure 1.1: Graphical representation of the Doppler shift from an object moving to the left[5].

Earth, and a transmitting satellite is put into orbit, the satellite will eventually pass overhead. If the observer were to record the frequency of the satellite as it passes overhead, they would measure a predictable Doppler shift in the received signal over the course of the pass.

A low-Earth orbit satellite pass can be divided into two characteristic phases. The first phase takes place from the time the satellite comes above the horizon to the time when it reaches its peak elevation. During this first phase, the satellite is moving towards a ground observer which causes a shift upward in the frequency of any transmissions. The second phase of the pass takes place from the point of peak elevation, to the time at which the satellite dips below the horizon. During this phase, the satellite is moving away from the observer, causing a shift lower in the frequency of any transmissions. The point which divides the two phases of the pass is the point at which the satellite reaches its peak elevation relative to the observer's location. At this point the satellite is essentially stationary relative to the observer, meaning that it is not moving radially with respect to the ground station. A cursory investigation of the data will clearly show this point, and it can be labeled the zero-crossing point of the data.

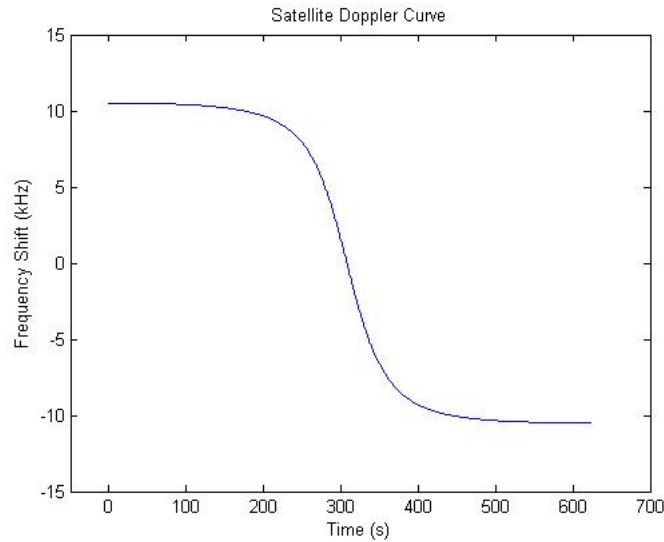


Figure 1.2: The Doppler curve produced from ground station observations of a passing LEO satellite.

Unless there are major thrusting maneuvers taking place during the interval of observation, the recorded Doppler curve is a continuous, smooth curve. Also, it is important to note that all frequency shifts recorded are only valid at the exact point where they were recorded. If another station were set up in a different location, the Doppler curve could be slightly different in shape, and the time of the observations would differ. Finally, one should note that the curve produced above would be significantly different if the satellite were in a different orbit.

## 1.2 Cube Satellite Standard

The CubeSat Project was started in 1999 at California Polytechnic State University with the primary mission of providing access to space for small payloads [17]. As a result of the project, costs for small businesses and academic institutions

have drastically shrunk. Further, with the development of the Poly Picosat Orbital Deployer (P-POD), cube satellite developers have been given an attractive fairing option which not only protects the cube satellite itself, but also ensures the safety of the launch vehicle and the primary payload.



Figure 1.3: Cube satellite payload fairing and deployment structure called the P-POD[7].

The CubeSat standard builds upon the development of the P-POD with a common form factor. A standard 1-U cube satellite is approximate 10 cm cube with a total mass of up to 1.333 kg[17]. The normal P-POD can launch up to three 1-U satellites. Additionally, designers can augment a satellite by adding additional cubes. One example is the Radiometric Atmospheric CubeSat Experiment (RACE) satellite, developed by the Texas Spacecraft Laboratory at the University of Texas-Austin, which uses a 3-U configuration.

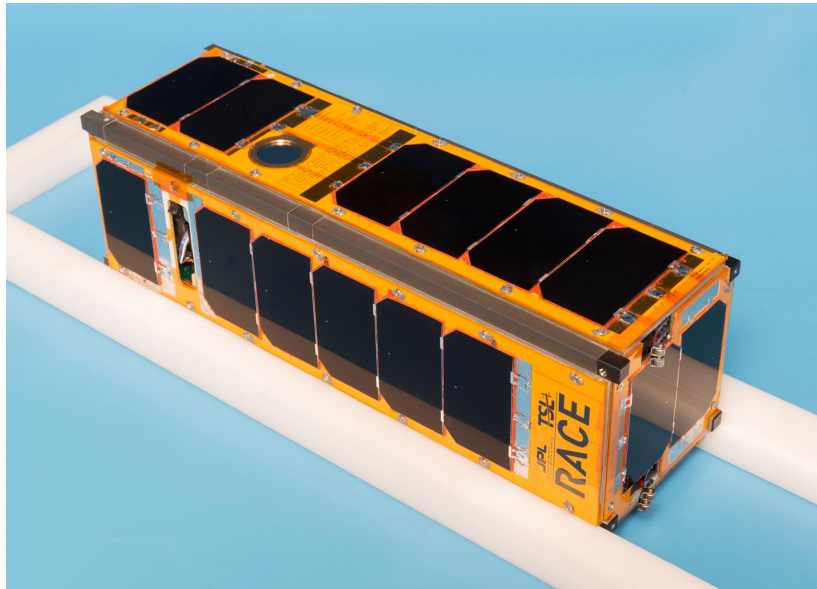


Figure 1.4: RACE satellite, created by the Texas Spacecraft Laboratory.

### 1.3 Background

Looking back to the beginning of the space age, the 1957 launch of Sputnik by the Soviet Union spurred engineers to develop a tracking method using Doppler frequency shift measurements. This method, developed and proven at the Applied Physics Laboratory, spurred the creation of the Navy Navigation Satellite System (NAVSAT), also called TRANSIT[9]. The TRANSIT system then became the first constellation of satellites used for navigation purposes. Now the GPS and other constellations have surpassed and replaced the original system, but the ability to use Doppler readings has persisted.

Tracking solutions for cube satellite missions is a growing challenge amongst academic research groups and amateur operators. For missions with margins allowing for a high fidelity GPS receiver, the challenge is one of initial acquisition and



re-acquisition. For missions of either case, the challenge spans the entirety of the mission. As the number of cube satellite missions increases, the number of low-cost missions without a GPS receiver will increase as well. Cube satellite missions of today are pushing the boundaries in terms of hardware capability and scientific breadth, and the driving force behind this movement is the push to lower technological costs and shorten timelines[19].

Mirroring the trend of cube satellites, ground stations are being designed to fit smaller budgets without sacrificing station abilities. Academic and private groups are developing designs and manuals emphasizing user-fabricated structures to support the professionally made required hardware. Meanwhile, software engineers and programmers are working to create generic station code, which can be modified and adapted for any purpose[10].

## **1.4 Contributions**

The goal of this thesis is to guide the reader through the technical knowledge and construction process of a low-cost satellite tracking system which can be operated from a single ground station if necessary. The tracking system exploits commonly available information and measurable frequency shift data to create a simple and continually updateable orbit model for any number of satellites. Additionally, the system is scalable to allow for combined efforts by amateur radio operators and other operational ground stations run by universities or interested parties. The tracking system allows for repeatable orbit model updates without use of GPS, for a wide range of orbits. Finally, an analysis is done of common low-earth orbits

in order to describe the levels of prediction error expected from certain propagators.

## **1.5 Thesis Organization**

This thesis is composed of eight chapters. Chapter 2 discusses the motivation behind creating a low-cost Doppler-based tracking system. Chapter 3 details each necessary component used by the tracking software and explains the background knowledge behind each component. Chapter 4 focuses on the hardware componentry of a ground station used for satellite tracking and communication and looks at ground operations. Chapter 5 contains the goals and procedures of mode 1 of the tracking software, a TLE-based pass prediction algorithm which provides nominal information for the main Doppler tracking system if necessary. Chapter 5 continues with mode 2, the main mode of orbit propagation and pass prediction. Mode 2 uses Doppler measurements to conduct post-processing and propagate predictions into the future. Chapter 6 discusses an analysis of the orbit model fidelity as time passes between relevant measured passes and studies the patterns of satellite passes for different inclinations. Chapter 7 presents the testing results for each mode of operation as well as the decision making process for specific situations. Finally, Chapter 8 concludes the thesis with thoughts and reflections on the tracking process and the possibility of expanded usage.

## **Chapter 2**

### **Motivation**

Remote sensing tasks, technology demonstrations, and biological experiments are a few examples of the many missions being undertaken in space using cube satellites[20]. With the push from industry and academia to expand the use of such small satellites to accomplish tasks, space hardware components have also shrunk in size, weight, and power in order to meet new mission requirements. However, many compromises are made when designing such a small satellite. In the case of the RACE mission, GPS receivers were not included to provide volume and mass for other scientific and guidance, navigation, and control (GN&C) hardware. This meant that in order to track the satellite, a GPS-independent tracking method had to be developed and employed. Otherwise, tracking would rely solely on publicly provided two-line element sets (TLEs). However, the TLE-based solution was potentially insufficient to meet mission requirements. Although the RACE mission for example, a mission that served as one of the primary motivations for this work, ended abruptly with the explosion of the Orbital Sciences Antares rocket in October of 2014[15], the work done here presents useable procedures and information for any other mission where tracking is required without the use of GPS.

This chapter focuses on the different motivations behind the push to create inexpensive yet robust methods of tracking the position and velocity of satellites

orbiting the Earth. The primary satellites of interest are not equipped with GPS receivers, and thus must rely on a different method to determine their location and predict their orbital motion. Additionally, satellites with GPS can still have use for this methodology in order to determine state vectors for ailing satellites, or to quickly determine the orbital position of the satellite after launch.

## **2.1 Primary Motivations**

As stated previously, the main reason that this work was necessary was to provide ground station operators for the RACE mission and other missions with a method of easily acquiring the position and velocity of their satellite and continuously tracking it over the duration of the mission. Without a GPS instrument aboard the flight unit the ground crew must rely on other methods of tracking. The following work would also help GPS-equipped satellites by providing additional tracking support.

Presently, there are two main methods of launching a cube satellite into Earth orbit. The first method is to purchase a secondary payload slot on a major launch vehicle[33]. For the second method, the satellite must be transported via a major launch vehicle to the International Space Station (ISS) prior to deployment. From there, the satellite is loaded into one of two deployment mechanisms, and deployed at a predetermined time[27]. In each case, the satellite's initial orbit is not known to a highly accurate degree. For ground operators this poses a problem of uncertainty in initial position. Should the ground operators not be able to identify their satellite's signal quickly among the group of secondary payloads, the

program developed in this thesis provides a number of methods to help acquire the satellite. The first method relies on the TLE tracker and propagator and is denoted as mode one. In addition to the TLE system, information could be used from the Doppler tracking method outlined in mode two in order to narrow down the orbit characteristics and help schedule upcoming passes.

## **2.2 Secondary Motivations**

Apart from primary needs met by this work, there is a necessity among small ground stations run by amateurs, universities, and even small private companies to keep fiscal costs low. The use of Doppler tracking allows operators to track their satellite using just the equipment already necessary to communicate with a satellite, thus keeping added costs to a minimum. The frequency shifts will be evident in the radio signal that the ground station receives. In order to measure and record these slight differences in the received signal, one can adapt the software defined radio system.

Another motivation for the work contained in this thesis is the ability to augment the coverage and tracking by incorporating data from multiple ground stations in the tracking task. This means that if another operator at a different ground station records the Doppler shift and employs the software, their observations could provide measurable improvements to the accuracy of the estimation. Using a connected network, different groups could provide constant tracking of any number of small satellites working together to ensure many small satellite missions are successful. Such a network of ground stations and operators would provide immense advan-

tages to all that decided to participate. More specifically, the enhanced coverage would increase total observations, more stations would allow for better geometry in the estimation problem, and overall more activity would increase the reliability of the system[31].

One final motivation for this work is that in some cases TLEs are improperly assigned to certain cube satellites, or contain significant errors in the orbit characteristics reported[11]. This can happen when a large number of cube satellites are deployed in a short period of time, yielding a “cloud” of small satellites with similar orbital parameters. Further, secondary payload slots on rocket launches can set cube satellites in orbits that are slightly different from what was originally expected. In terms of propagation, using a simplified perturbations model, such as the SGP4 method of orbit propagation, alone will result in errors on the order of a few kilometers to tens of kilometers depending on the time from epoch[30]. The Doppler method would incrementally help correct this problem and would provide users with a solution for their continuous tracking needs.

## **Chapter 3**

### **Technical Components**

When constructing a satellite tracking system for use with ground station hardware, there are many different concepts that must be considered. The satellites of interest all exhibit motion most closely defined by the classical Keplerian orbit element set, but in the real space environment of low-Earth orbit there are many perturbations, both conservative and non-conservative, that must also be considered in order to create a more accurate model. Further, beyond simply characterizing the orbit of a satellite, one must define the motion with respect to multiple different frames of reference. For instance, if the motion has been defined in an inertial sense, in order to compute the state vector representation of the satellite's motion with respect to a location on the ground, many conversions must be made. Finally, the concepts of time must be considered along with numerical integrators in order to be practically combined to produce useable orbit tracks.

This chapter briefly overviews all of the different fundamental concepts and tools involved in satellite tracking and orbit propagation.

#### **3.1 Reference Frames**

There are a number of necessary reference frames and position representations needed in order to calculate the absolute and relative positions of a satellite

moving in orbit. This section briefly discusses each relevant frame used in the operation of a ground station.

### **3.1.1 Orbital Elements**

The most common form of the orbital elements is the traditional form, often referred to as the Keplerian form. This form is named after Johannes Kepler, who created the three laws of planetary motion. According to Kepler, if a simple system is defined as two objects, a large primary and a relatively small secondary body, then the motion will be perfectly described by a single set of elements[2].

There are six variables which compose the orbital element set. In a perfect 2-body case, the first five remain constant while the last is either denoted as the fast moving variable, or given as an initial value at some epoch. The eccentricity defines how elliptic the orbit is, meaning that if the orbit were perfectly circular it would have an eccentricity of zero. The semi-major axis gives a characterization of the orbit size. It is defined as the sum of the apoapsis and periapsis distances divided by two. The inclination is defined as the angle that the satellite's orbit plane makes when the satellite crosses the equator moving northward. The longitude of the ascending node is defined as the angle between the point at which the satellite crosses the equatorial plane moving northward and the reference x-axis direction. The argument of periapsis dictates the orientation of the orbit within the orbit plane, and is defined as the angle between the ascending node and the periapsis point.

The sixth variable is the fast moving variable, and it is one of three angles: the true anomaly, the eccentric anomaly, or the mean anomaly at some defined epoch. Each one serves the purpose of describing the position of the orbiting



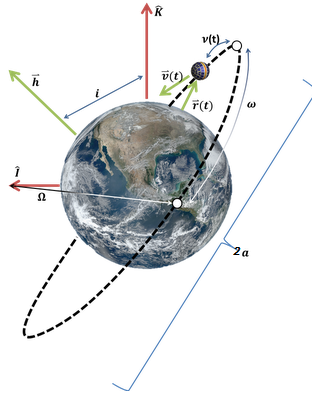


Figure 3.1: Graphical representation of the orbital elements for a typical orbit[13].

body as it moves through a Keplerian orbit, though each describes this position in a slightly different way. The true anomaly is the angle between the periapsis point and the orbiting body, drawn from the foci where the primary body presides, at any given time. The eccentric anomaly is another angular element, except unlike the true anomaly, it is drawn from the geometric center of the orbit. Also, the eccentric anomaly is aligned by drawing a perpendicular to the eccentricity vector, which also intersects the orbiting body. The point at which this perpendicular line intersects a surrounding circle corresponds to the point at which the angle is measured. Finally, the mean anomaly relates to the amount of area swept out by the orbit when drawing a line from the primary foci to the circumscribing circle, which is drawn around the orbiting body. The mean anomaly increases uniformly from 0 to  $2\pi$ .

### 3.1.2 Earth-Centered Inertial Frame (ECI)

The Earth-centered inertial coordinate frame is set with an origin at the center of mass of the Earth. The I-axis for this frame is pointed in the direction of the vernal equinox. The K-axis is set to correspond to the Earth's rotation axis, which

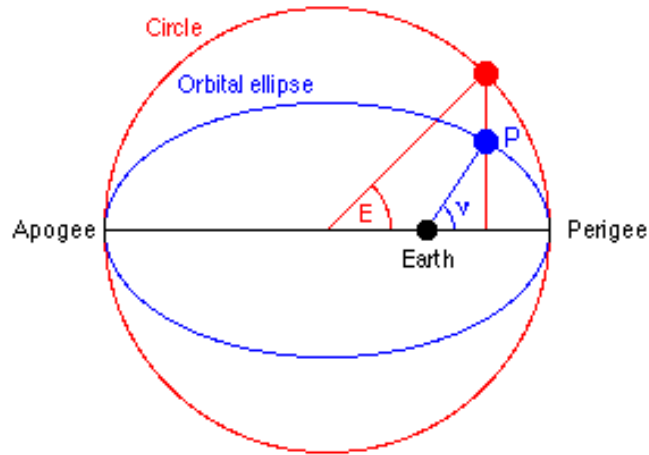


Figure 3.2: Graphical representation of true anomaly compared to eccentric anomaly for an orbiting satellite[18].

is also perpendicular to the equatorial plane. Finally, the J-axis completes the right-handed set. In order to be defined as inertial, the frame must not be accelerating. In the case of the Earth, it is clear that there are accelerations, since the Earth orbits the Sun. This means that this frame is not truly inertial, but more of an inertial-like frame. For the sake of this analysis, the durations of time are small enough that the assumption of this frame being inertial is allowed.

### 3.1.3 Earth-Centered Earth-Fixed Frame (ECEF)

The Earth-centered Earth-fixed coordinate frame also has its origin set at the Earth's center of mass, but unlike the inertial frame, its axes rotate with the Earth. This means that the axes point to specific locations of the Earth's surface, rather than a set point in space. The i-axis points to  $0^\circ$  Latitude and Longitude. The Earth's prime meridian, or line of  $0^\circ$  Longitude, is defined to pass through Greenwich, England. The plane of  $0^\circ$  Latitude is known as the equator. The k-axis points in the

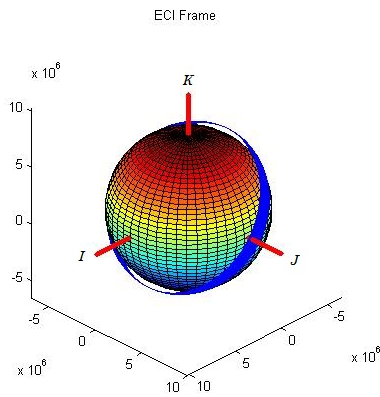


Figure 3.3: Satellite orbit viewed in the ECI frame. Axes are aligned with the celestial sphere and do not rotate with the Earth.

direction of the Earth's rotation axis. Finally, the j-axis completes the right-handed set. It is worth noting that at any given time, the k-axis may not correspond directly with the Earth's geometric pole due to the gyroscopic procession of the pole.

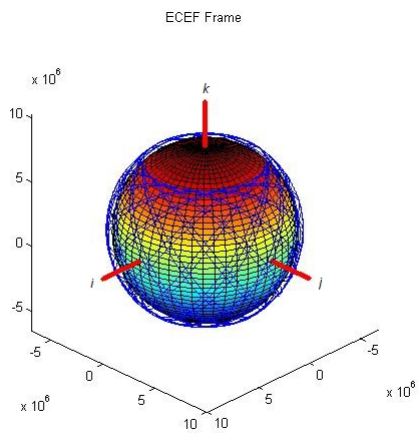


Figure 3.4: Satellite orbit viewed in the ECEF frame. Axes rotate with the Earth allowing major movements relative to the Earth's surface to be seen.

### 3.1.4 Topocentric Frames

Topocentric coordinate frames differ from the ones previously discussed because their origins lay on the surface rather than at the center of mass. They are not constrained to one single origin, but rather, are placed wherever is most convenient for a particular application. Two common systems are the East-North-Up (ENU) coordinate frame and the South-East-Zenith (SEZ) coordinate frame. Both are right-handed orthonormal sets which can be used in coordination with other sets previously mentioned.

Topocentric frames provide a unique reference frame that allows objects to be coordinated in a frame that is centered on a user. For ground station operators, the frame is centered on the antennas. This provides the most convenient perspective for any conversions to be done. For satellite communications, the most manageable form of expressing the direction of a satellite is to use angles which are set at the origin of the ENU topocentric frame. The two angles needed are azimuth, defined as the deviation from north, and elevation, defined as the angle from the horizon towards the zenith. By using this common topocentric frame, operators are able to use these measures to control the antenna pointing direction. For the work done here, the ENU coordinate frame, along with the azimuth and elevation defined above, were used to provide satellite tracks for antenna controllers. Additionally, the elevation angle provided a convenient metric by which to determine when a satellite was passing overhead. For the research done here, the SEZ set was used to denote the range and range-rates of the satellite.

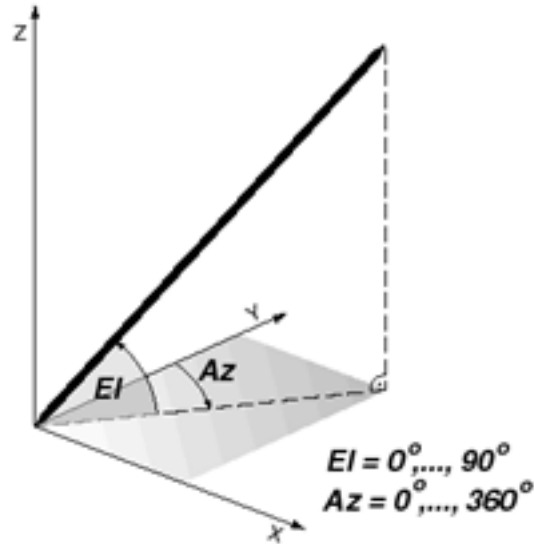


Figure 3.5: Antenna pointing with associated direction angles aligned in the ENU frame[23].

### 3.1.5 Geocentric & Geodetic Coordinates

In geocentric coordinates the Earth is assumed to be a sphere. The origin of the system is set at the geometric center of the Earth, which is also assumed to be the center of mass. In order to determine the location of an object, angles are drawn with reference to a direction from the center of the Earth. This reference is set at  $0^\circ$  Latitude and Longitude. Lastly, the radial location of an object in this system could be given in a total radius from the origin or an altitude above the defined surface depending on the application.

In geodetic coordinate systems, the Earth's shape is approximated by ellipsoid. Specifically, the oblate spheroid is used to represent the Earth with a flattening at the poles and a bulge at the equator. The origin of the system is set as the center of

mass of the Earth. The longitude of an object is determined similarly to that of the geocentric system, but the latitudes differ. For geodetic coordinates, the latitude of an object is defined as the angle between the local normal or zenith direction, and the equatorial plane. Due to the different definitions, a single location will yield different latitudes based on the system one decides to use. In order to determine the radial location of an object in this system a height above the reference ellipsoid is given. There are many different geodetic systems in use today. The system used in this research is the World Geodetic System 1984 or WGS84.

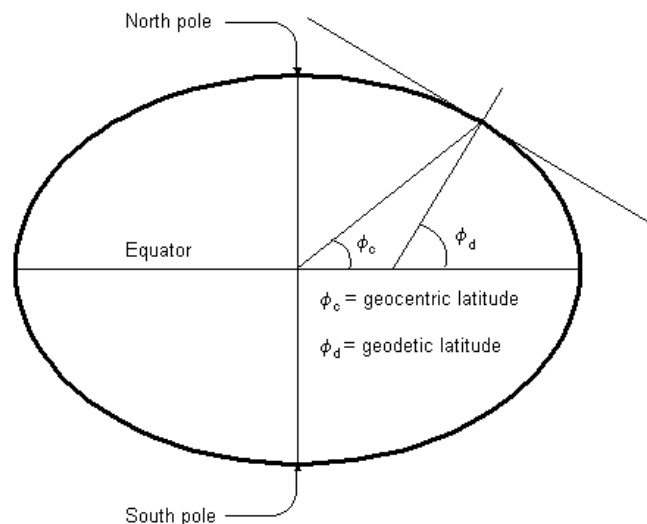


Figure 3.6: Graphical representation of the difference between geocentric latitude and geodetic latitude[8].

### 3.2 Conversions

In order to do orbit predictions and operate a ground station, a number of conversions are required. These conversions allow the prediction and tracking pro-

gram to quickly move through different frames and display results in a useful manner, both for the user and the control software. This section discusses the conversions between each relevant frame.

### 3.2.1 Conversion of a State Vector to Orbital Elements

The conversion from a state vector representation of a satellite's position to the corresponding orbital elements is an instantaneous 1:1 mapping. This means that for any state vector, there is a unique set of orbital elements. These orbital elements describe a perfect Keplerian orbit, so regardless of what perturbations may affect the satellite's movement, the resulting orbital elements will only describe the Keplerian orbit that would follow if those perturbations did not exist. The following formulas describe the conversions from a position and velocity state vector to the orbital elements. The results in the next few pages are found in many textbooks and are repeated here for completeness and later reference. The inertial position and velocity vectors are given by the following expressions.

$$\vec{\mathbf{r}} = x\hat{\mathbf{i}} + y\hat{\mathbf{j}} + z\hat{\mathbf{k}} \quad (3.2.1)$$

$$\vec{\mathbf{v}} = \dot{x}\hat{\mathbf{i}} + \dot{y}\hat{\mathbf{j}} + \dot{z}\hat{\mathbf{k}} \quad (3.2.2)$$

After defining the position and velocity vectors one must use that information to describe the orientation of the orbital plane in three-dimensional space. This is done by calculating the angular momentum vector and the eccentricity vector. The eccentricity is simply found by taking the norm of its vector.

$$\vec{\mathbf{h}} = \vec{\mathbf{r}} \times \vec{\mathbf{v}} = h_x \hat{\mathbf{i}} + h_y \hat{\mathbf{j}} + h_z \hat{\mathbf{k}} \quad (3.2.3)$$

$$h = \|\vec{\mathbf{h}}\|$$

$$\vec{\mathbf{e}} = \frac{\vec{\mathbf{v}} \times \vec{\mathbf{h}}}{\mu} - \hat{\mathbf{r}} \quad (3.2.4)$$

$$e = \|\vec{\mathbf{e}}\|$$

Additionally, the normal vector is calculated. Although it is not an orbital element itself, the normal vector is important in defining the argument of perigee and the right ascension of the ascending node.

$$\vec{\mathbf{n}} = \hat{\mathbf{k}} \times \vec{\mathbf{h}} = n_x \hat{\mathbf{i}} + n_y \hat{\mathbf{j}} + n_z \hat{\mathbf{k}} \quad (3.2.5)$$

$$n = \|\vec{\mathbf{n}}\|$$

At this point, the remaining orbital elements are calculated using the following formulas. For the argument of perigee, the right ascension of the ascending node, and the true anomaly calculations must be done in order to determine the correct quadrant.

$$a = \frac{h^2}{\mu(1 - e^2)} \quad (3.2.6)$$

$$i = \cos^{-1}\left(\frac{h_z}{h}\right) \quad (3.2.7)$$

$$\omega = \begin{cases} \cos^{-1}\left(\frac{\vec{\mathbf{n}} \cdot \vec{\mathbf{e}}}{ne}\right) & \text{if } \vec{\mathbf{e}} \cdot \hat{\mathbf{k}} > 0 \\ 2\pi - \cos^{-1}\left(\frac{\vec{\mathbf{n}} \cdot \vec{\mathbf{e}}}{ne}\right) & \text{if } \vec{\mathbf{e}} \cdot \hat{\mathbf{k}} < 0 \end{cases} \quad (3.2.8)$$



$$\Omega = \begin{cases} \cos^{-1}\left(\frac{n_x}{n}\right) & \text{if } \vec{n} \cdot \hat{\mathbf{j}} > 0 \\ 2\pi - \cos^{-1}\left(\frac{n_x}{n}\right) & \text{if } \vec{n} \cdot \hat{\mathbf{j}} < 0 \end{cases} \quad (3.2.9)$$

$$\nu = \begin{cases} \cos^{-1}\left(\frac{\vec{r} \cdot \vec{e}}{re}\right) & \text{if } \vec{r} \cdot \vec{v} > 0 \\ 2\pi - \cos^{-1}\left(\frac{\vec{r} \cdot \vec{e}}{re}\right) & \text{if } \vec{r} \cdot \vec{v} < 0 \end{cases} \quad (3.2.10)$$

### 3.2.2 Conversion of Orbital Elements to a State Vector

The conversion from the orbital elements to a position and velocity state vector takes place in three phases. First, depending on which anomaly has been given, the user must convert the give value to a true anomaly form so that the direct mapping may proceed. This involves using Kepler's equation to iterate and find the correct value for the true anomaly. Kepler's equation is shown below.

$$M = E - e \sin(E) \quad (3.2.11)$$

In order to solve the equation, one must iterate using the following equation to find a solution. For the first iteration, simply assign  $E^* = M$  and proceed with the algorithm using the update formula.

$$\Delta E = \frac{M - E^* + e \sin(E^*)}{1 - e \cos(E^*)} \quad (3.2.12)$$

$$E^* = E^* + \Delta E \quad (3.2.13)$$

Apart from manually solving the equation through iteration, there are many functions built into different programming languages that will help to solve the

equation in a single line of code. Once the user has solved for the eccentric anomaly, the next step is to solve for the true anomaly using the following formula. Once the user has the true anomaly, the rest of the conversion process proceeds.

$$\tan\left(\frac{\nu}{2}\right) = \tan\left(\frac{E}{2}\right) \sqrt{\frac{1+e}{1-e}} \quad (3.2.14)$$

At this point, work is done in a perifocal, or two-dimensional, frame. This perifocal frame provides a convenient way to define the size and shape of the orbit without worrying about the orientation in three-dimensional space. Once the characteristics are in place, the perifocal state vector is derived. This yields the exact two-dimensional orbit that is described by the elements without any orientation assignments.

$$p = a(1 - e^2) \quad (3.2.15)$$

$$r = \frac{p}{1 + e \cos \nu} \quad (3.2.16)$$

$$\vec{\mathbf{r}}_{pqw} = \begin{bmatrix} r \cos(\nu) \\ r \sin(\nu) \\ 0 \end{bmatrix} \quad (3.2.17)$$

$$\vec{\mathbf{v}}_{pqw} = \sqrt{\frac{\mu}{p}} \begin{bmatrix} -\sin(\nu) \\ e + \cos(\nu) \\ 0 \end{bmatrix} \quad (3.2.18)$$

Finally, three successive rotations are done using the remaining elements in order to properly align the orbit in three-dimensional space. An Euler sequence

detailed below consisting of three consecutive simple rotations properly places the final orbit plane and yields the final state vector.

$$\vec{\mathbf{r}} = \mathbf{R}_{313}(-\omega, -i, -\Omega)\vec{\mathbf{r}}_{pqw} \quad (3.2.19)$$

$$\vec{\mathbf{v}} = \mathbf{R}_{313}(-\omega, -i, -\Omega)\vec{\mathbf{v}}_{pqw} \quad (3.2.20)$$


| <u>Orbital Elements</u> |  | <u>State Vector</u>                |
|-------------------------|--|------------------------------------|
| a = 7200 km             |  | $r_x = 1.994086035 \times 10^3$ km |
| e = 0.01                |  | $r_y = 5.976639570 \times 10^3$ km |
| i = 48°                 |  | $r_z = 3.333641131 \times 10^3$ km |
| $\omega = 36^\circ$     |  | $v_x = -4.670969491$ km/s          |
| $\Omega = 80^\circ$     |  | $v_y = -3.975729424$ km/s          |
| v = 3°                  |  | $v_z = 4.342082673$ km/s           |

Figure 3.7: Orbital elements and the instantaneous corresponding state vector.

### 3.2.3 Conversion From ECI to ECEF

For the conversion between the ECI and ECEF reference frames, the following expression contains the rotation matrices for the precession of the node, nutation of the node, rotation of the Earth, and polar motion.

$$\vec{\mathbf{r}}_{ECEF} = R_M R_S R_N R_P \vec{\mathbf{r}}_{ECI} \quad (3.2.21)$$

In order to simplify this expression, one must first look back at the assumptions made about each system. For this analysis the polar motion, precession, and

nutations are ignored due to their slow-changing nature. For this program predictions and tracking will be continuously done every day, leaving the Earth's rotation as the only major rotation required[29]. This allows for a much simpler form of the conversion using a single rotation, where the rotation is done about the Earth's axis of rotation, which is also assumed to correspond to the geometric axis. The conversion is given by the following formula.

$$\vec{\mathbf{r}}_{ECEF} = \begin{bmatrix} \cos(\Theta) & \sin(\Theta) & 0 \\ -\sin(\Theta) & \cos(\Theta) & 0 \\ 0 & 0 & 1 \end{bmatrix} \vec{\mathbf{r}}_{ECI} \quad (3.2.22)$$

The angle about which the rotation is done is noted as a sum of the Greenwich Mean Sidereal Time (GMST) and Earth's rotation rate multiplied by the time since epoch.

$$\Theta(t) = \Theta(t_0) + \omega_E t \quad (3.2.23)$$

In the case of an offset angle between the K and k axes, formula 3.2.23 would need to be augmented with other rotations in order to compensate for the offset angle.

### 3.2.4 Conversion Between ECEF and Topocentric Frames

The conversion between the ECEF reference frame and any topocentric reference frame is simply an Euler sequence or a sequence of simple rotations. In the case of the SEZ reference frame the conversion from ECEF to SEZ is a 3-2 rotation sequence over the longitude and 90°-latitude respectively. The conversion is given below.

$$\vec{\mathbf{r}}_{SEZ} = \mathbf{R}_{32}(90-\varphi, \lambda) \vec{\mathbf{r}}_{ECEF} \quad (3.2.24)$$

Combining the equations to form a single rotation matrix yields the following conversion.

$$\vec{\mathbf{r}}_{SEZ} = \begin{bmatrix} \cos(90-\varphi) \cos(\lambda) & \cos(90-\varphi) \sin(\lambda) & -\sin(90-\varphi) \\ -\sin(\lambda) & \cos(\lambda) & 0 \\ \sin(90-\varphi) \cos(\lambda) & \sin(90-\varphi) \sin(\lambda) & \cos(90-\varphi) \end{bmatrix} \vec{\mathbf{r}}_{ECEF} \quad (3.2.25)$$

In order to convert back from the topocentric frame into the ECEF reference frame one simply inverts the rotation matrix and proceeds.

### 3.2.5 Conversion from ECEF to LLH

In order to convert from ECEF coordinates to geodetic latitude, longitude, and height above the ellipsoid (LLH), one must first consider the system being used. As stated before, this research uses WGS84, so all calculations will account for this ellipsoid model only. The following are parameters defining the ellipsoid.

$$R_E = 6378137.0m$$

$$R_P = 6356752.314m \quad (3.2.26)$$

$$f = \frac{(R_E - R_P)}{R_E} = 0.003352810$$

Next, a set of initial calculations are done in order to yield results that will be used later in the conversion process.

$$R_P = R_E(1 - f)$$

$$e = \sqrt{\frac{(R_E^2 - R_P^2)}{R_E^2}} \quad (3.2.27)$$

$$e_P = \sqrt{\frac{(R_E^2 - R_P^2)}{R_P^2}}$$

These initial calculations use characteristics of the Earth along with the ECEF position of the object to begin incorporating the non-spherical model when describing the object's true position.

$$p = \sqrt{x_{ECEF}^2 + y_{ECEF}^2} \quad (3.2.28)$$

$$\theta = \tan^{-1}\left(\frac{z_{ECEF}R_E}{pR_P}\right) \quad (3.2.29)$$

Now, the geodetic latitude and longitude are calculated using the following formulas. This method does not use iteration in order to find the result.

$$\phi_{Geodetic} = \tan^{-1}\left(\frac{z_{ECEF} + e_P^2 R_P \sin^3(\theta)}{p - e^2 R_E \cos^3(\theta)}\right) \quad (3.2.30)$$

$$\lambda = \tan^{-1}\left(\frac{y_{ECEF}}{x_{ECEF}}\right)$$

Finally, the height above the ellipsoidal surface is calculated.

$$N_h = \frac{R_E}{\sqrt{1 - e^2 \sin^2(\phi_{Geodetic})}} \quad (3.2.31)$$

$$H = \frac{p}{\cos(\phi_{Geodetic})} - N_h$$

For additional reference, one can calculate the geocentric latitude of any object using the following formula. Note that the geocentric longitude is the same as the geodetic longitude due to the Earth ellipsoid model being an oblate spheroid.

$$\phi_{Geocentric} = \sin^{-1}\left(\frac{z_{ECEF}}{r_{ECEF}}\right) \quad (3.2.32)$$

One of the main purposes for using this conversion and finding the geodetic coordinates of the object in orbit is to visualize the orbit on a two-dimensional chart. The chart can be used as a reference to monitor the orbit, the satellite's location, or simply as a check for insuring that conversion results correspond with the expected location.

### **3.3 Dynamical Models & Numerical Integration**

In the case of orbit propagation, numerical integrators provide a means of applying dynamical equations of a specific system to find the position and velocity of a spacecraft given a set of initial conditions and a time of integration. There are many different numerical integrators available for use, but for this research the ode45 integrator built into Matlab was used. This section is focused on the dynamical models used to generate the equations of motion which serve as the basis for the numerical integrator.

#### **3.3.1 J2 Perturbation Model & Integration**

When modeling the Earth's gravitational field, the requirements of the mission dictate how accurate the model must be. As the need for accuracy increases,

perturbations of higher degree and order must be accounted for in the model. Also, depending on the time of flight being considered, moving to a higher degree and order model may be needed to continue satisfying mission requirements. In the case of this program however, the gravity model includes the dominating two-body term and the Earth's  $J_2$  term. The Earth is an oblate spheroid, and thus contains a significant  $J_2$  term which dominates the non-spherical gravity perturbations[12]. Overall, a spacecraft in low-Earth orbit (LEO) will be greatly influenced by the  $J_2$  term, causing movement in the longitude of the ascending node. Due to the significance of this effect, the  $J_2$  perturbation alone was included in the dynamical model.

In order to create the gravity model for the system, first a gravitational potential equation was made. The equation includes the potential due to the two-body term and the potential term due to Earth's  $J_2$  term. Next, partial derivatives are taken of the expression of the gravitational potential in order to describe the Cartesian forces that would be felt by a spacecraft in this environment.

$$U = \frac{\mu}{r} - \frac{\mu}{r} \left(\frac{R}{r}\right)^2 J_2 \left(\frac{3}{2} \left(\frac{z}{r}\right)^2 - \frac{1}{2}\right) \quad (3.3.1)$$

$$r = \sqrt{x^2 + y^2 + z^2}$$

Finally, a system of equations called the linearized equations of motion was created. These expressions, along with a set of initial conditions, are what will be input into the ode45 function in order to proceed with the numerical integration.



$$\begin{aligned}
\dot{x} &= v_x \\
\dot{y} &= v_y \\
\dot{z} &= v_z \\
\ddot{x} &= \frac{dU}{dx} \\
\ddot{y} &= \frac{dU}{dy} \\
\ddot{z} &= \frac{dU}{dz}
\end{aligned}
\tag{3.3.2}$$

### 3.3.2 Drag Model & Integration

Modeling the forces of drag felt by an orbiting satellite is a challenge in the LEO environment. First, the atmospheric model selected to be used is not necessarily accurate. In most cases the model is simply a set of formulas or table values discretized in order to mimic empirical data previously measured by other missions at varying altitudes. Research into the atmospheric drag felt in LEO started many years ago and has continued today with missions such as the Drag and Atmospheric Neutral Density Explorer[25]. These missions seek to accurately measure the forces felt on a satellite due to atmospheric drag, and they drive the atmospheric models of today. No single atmospheric model has proven itself to be accurate in all cases, but each contains strengths and weaknesses[32]. For the purposes of this research, a distinction must be made when considering drag.

If a spherical satellite is sent to LEO, it will experience a force due to atmospheric drag. This force can be modeled as being wholly in the anti-velocity direction. For satellites that are non-spherical however, the force is not so evenly

distributed. In many cases a differential, or uneven, force is felt by the satellite. These differential forces can cause changes in attitude and, more severely, satellite tumbling. In this case of differential forces, modeling the dynamics is potentially very complex. For this reason, differential forces due to drag are not considered any further in this research.

Using the idea of the drag force acting only in the direction opposite to that of the velocity along with a number of other assumptions allows engineers to create a simple model of the drag force felt by the satellite. The first assumption is that the atmosphere rotates as the Earth rotates. It is important to note that the force felt by the satellite is due to the relative motion of the satellite with respect to the atmosphere, rather than simply the motion of the satellite[12]. The relative motion of the satellite is then stated as the following.

$$\vec{v}_{rel} = \vec{v} - \vec{\omega}_E \times \vec{r} \quad (3.3.3)$$

From here, one references the following equation for the acceleration felt due to drag. This formula requires the atmospheric density which is found using a standard atmospheric model, as well as the ballistic coefficient of the satellite. The ballistic coefficient is also defined below and involves the mass, cross-sectional area, and drag coefficient of the satellite. Finally, the expression for the acceleration due to drag is shown below.

$$\vec{a} = -\beta \rho v_{rel} \vec{v}_{rel} \quad (3.3.4)$$

In order to reduce the complexity of the program and the overall need for more operator input, drag has not been included in the tracking program's integration scheme. As such, all results generated in this thesis were produced in the absence of an atmospheric model. Should the need arise for a more accurate state vector solution, an atmospheric model and the subsequent forces it produces can be implemented into the integration scheme with little effort. Beneath ISS orbit, it has been shown that drag can produce significant perturbations over long periods of time, even to the point of using mechanical structures to force a state of aerodynamic stability[22]. However, for this purpose, and in the absence of a set satellite structure model, the drag forces have been disregarded.

### **3.4 Time Systems**

Time is one of the most important components needed for tracking a satellite or network of satellites. For this research, it was important to understand a number of time systems so that data could be interpreted correctly, measurements could be stamped accurately, and proper comparisons could be made. In this section some relevant time systems that are used later in the tracking program are briefly discussed.

#### **3.4.1 Julian Date & Modified Julian Date**

The Julian date (JD) is defined as the number of mean solar days that have passed since noon of January 1st 4713 B.C. The modified Julian date (MJD) is defined as the number of mean solar days that have passed since midnight on November 17th, 1858. This corresponds to exactly 2400000.5 days after the Julian day 0.

It is also worth noting that by adding 0.5 to the date, the modified Julian date begins at midnight instead of noon. When converting between the two, this distinction must be taken into account.

### **3.4.2 Unix Time**

Unix time is a system that describes the exact number of seconds that have passed since 00:00:00 Coordinated Universal Time (UTC) of January 1st, 1970. This system does not count leap seconds. The reason that this system of time is important to this tracking program is that the computers which run the ground station at the Texas Spacecraft Laboratory run the Unix operating system, and thus Unix time is a convenient method for tagging predictions and observations. Unix time is the primary time system used for satellite tracking in this program.

## **Chapter 4**

### **Ground Station Construction and Operations**

Cube satellite radio communications are primarily contained within the amateur radio frequency bands. For the RACE mission, the bands of interest were 144-146 MHz for the uplink from the ground station to the satellite, and 435-438 MHz for the downlink from the spacecraft to the ground. The main goal of the communication hardware both on the satellite and on the ground was to ensure information could be transferred at the required rates between the ground station and the satellite. Without proper communication hardware selections, the radio frequency links can never be made, deeming the mission a failure.

This chapter briefly discusses the hardware componentry involved in constructing and using a ground station designed for radio frequency communication within the amateur radio band. Specifically, the chapter will focus on the hardware configurations used in the Texas Spacecraft Laboratory ground station. Finally, the chapter will overview the advantages of implementing a Doppler tracking system on the selected hardware.

#### **4.1 Hardware**

There are a number of hardware pieces that compose the main functions of a satellite ground station. As stated in the introduction, the bands of interest for this

ground station were the amateur radio bands in the frequencies ranges mentioned earlier. Due to these required operating ranges, the hardware was selected to ensure peak performance within the amateur bands. Also, by selecting components that can operate effectively within the entire amateur radio band, support for future cube satellite missions is guaranteed. Overall, the components needed were antennas, amplifiers, pre-amplifiers, cabling, software-defined radios, and computer stations to control the operation[14].

#### **4.1.1 Computers & Software-Defined Radios**

Two primary ground station computers control the antennas and radios, guiding the system. For the radios, software-defined radios were used because of the flexibility in their performance and capabilities. Software-defined radios provide a unique platform for programming, testing, and continued usage in many different scenarios[16]. The radios handle all of the phases of turning the digital command from the computer into an analog radio frequency signal and then outputting that signal to the amplifiers. For the software-defined radios however, the power output is not sufficient to be directly put into a high power amplifier. In order to get power levels for the uplink to the specified level, an intermediate amplifier must be used in addition to the high power amplifier.

#### **4.1.2 Amplifiers**

In the case of the uplink, two amplifiers were set up in order to increase the signal power for commanding transmissions. The intermediate power amplifier increases the output from the software-defined radio from 30mW to roughly 4W.

Then, the signal was amplified by a high power amplifier to approximately 160W. At this point the signal was sent directly to the uplink antenna for transmission. Both power amplifiers were given dedicated power supplies to ensure operation in linear regime.

For the receiving signal, a preamplifier was mounted on the antenna mast in order to amplify the low power signal received from the satellite while not significantly increasing the noise levels within the signal. Amplifying the signal at the immediate point of reception is important in order to preserve and even increase signal to noise ratios and ensure that the information within the signal can be received properly. This preamplifier was powered remotely using a bias tee which provided DC power without interfering with the high frequency radio signal.

### **4.1.3 Antennas**

The antennas that were selected were high-gain, directional yagi antennas and each antenna was mounted with pointing control rotors. The uplink antenna was chosen not only because it supports radio transmission between 144-148MHz, but also because it provides a gain of 14.39dBic while still having a relatively wide beamwidth of 38°. This antenna would be used for commanding satellites, so any margin that could be gained on the uplink budget was preferable. For the downlink, an antenna which operates in the range of 430-438MHz was chosen in order to receive communications from satellites in the amateur radio band. This antenna was also chosen because of the 18.9dBic gain it provides, while having a narrower beamwidth of 21°. For the downlink, the margin is smaller for communications. This is due to the fact that cube satellites do not have large power budgets to devote

to communications, and further, do not have the structural ability to mount a larger antenna for higher gain transmissions. In order to ensure adequate margins for the required communication rates, the receiving antenna required higher directionality and increased gain. In order to ensure these required levels were met, the antenna is nearly 19 feet long.



Figure 4.1: Mounted Antennas used by the Texas Spacecraft Laboratory.



#### **4.1.4 Cabling**

The final major component involved in the system was the cabling from the roof installation to the ground station control room. Appropriate cabling is an important factor in ground stations for a number of reasons; extensive cabling can potentially cause power losses and increased noise in a radio signal. Secondly, for the uplink in particular, the cabling must be an adequate thickness in order to handle potentially high power electrical signals. For the ground station at the Texas Spacecraft Laboratory, 400 series coaxial cable was selected and installed directly through specific access ports in order to minimize the total cable length needed.

Cables were also built for the amplifier power supplies. Each wire was selected to meet required standards based on the voltage and current levels expected to be pulled by the relevant power supply. This was done to ensure the safety of the station as well as ensure that performance levels could be achieved when required[3].

## **4.2 System Configurations**

Ultimately, the system at the Texas Spacecraft Laboratory was built for communication with cube satellites in amateur radio frequency bands. The design and construction of the system met those needs.

### **4.2.1 Ground Transmission System**

In the uplink portion of the ground station there are three major phases of the system handled by a number of different components. First, the digital information

encoded in the command message is inputted into the software-defined radio where it is converted to an analog signal for transmission. Next, the signal power level is greatly amplified in order to ensure it will be received at the specified bit rate. Finally, it is transmitted via the VHF yagi antenna. A diagram of the entire system is shown in Figure 4.2.1.

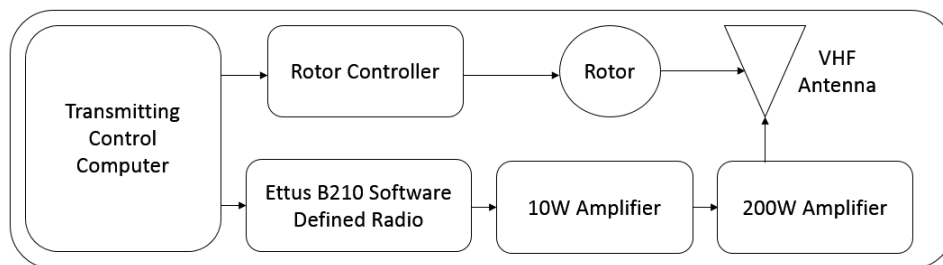


Figure 4.2: System Diagram for the transmitting portion of the ground station.

## 4.2.2 Ground Receiving System

In order to receive a downlinked message from the satellite, a separate system was created to meet the unique needs of this task. Again, there are three main phases of the process. In the first phase, a communication signal is received by the UHF antenna. This received signal is of very low power due to the losses in free space transmission. Due to this, the second phase involves amplification and filtering. When done properly using a pre-amplifier, this boosts the signal-to-noise ratio. By boosting the signal, the final phase is able to commence. The signal is converted back from analog to digital on the software defined-radio and decoded on the computer. A full diagram of the system is displayed in Figure 4.2.2.

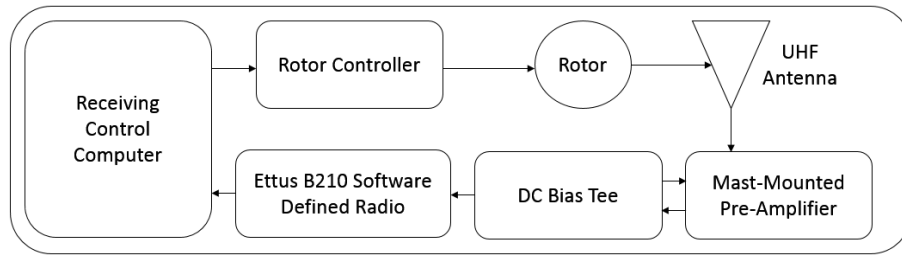


Figure 4.3: System Diagram for the receiving portion of the ground station.

### 4.3 Doppler Tracking Hardware Advantage

Using the ground system described previously, operators can use mode one of the tracking program described later in this thesis to acquire the position and velocity of a LEO cube satellite and schedule ground pass operations. Then, they can continuously update the orbit, generate pass predictions, and communicate with their cube satellite. With only the hardware required in order to run a normal ground station, operators can also handle the tracking and monitoring of their satellite in the terms of scheduling and maintenance.

There are two main methods of conducting Doppler investigations for cube satellites. The first requires a function generator, a multiplexer, a low-pass filter, and a spectrum analyzer. For this method, engineers must replicate the known transmitting carrier signal in order to multiplex it with the received signal. Then after passing the resulting signal through the low-pass filter, operators can observe the Doppler signal on a spectrum analyzer. This method results in a more precise measurement of the instantaneous doppler shift[24]. The method suggested for use with this ground system suggests indirectly measuring the Doppler shift. The received signal is measured in the software-defined radio as the instantaneous received fre-

quency. Next, the value is subtracted from the known transmitting frequency, and labeled as the Doppler shift. This method will not be as accurate when one considers the probabilistic qualities of the equipment but is sufficient for this analysis. In order to incorporate the probabilistic effects of the frequency generator within the flight transmitter, a system identical to the hardware on flight would be run at the ground station, and the frequency observed there would be subtracted instead of just the assigned frequency. When a frequency generator runs for extended periods of time, the stability of the oscillators becomes a factor of concern. Small random deviations in the oscillators will cause small random shifts in the frequency of the signal produced. By running an identical frequency generator on the ground, operators can more readily take these random deviations into account, allowing for a more accurate assessment of the Doppler shift.

These techniques are advantageous because they allow mission operations to continue without the help of outside resources. Ground station operators have the option to use external resources for tracking help, but ultimately it is not necessary. Furthermore, using this method, the tracking and scheduling can be done internally without the use of a flight GPS unit.

Finally, small scale cube satellite missions are an attractive gateway for universities, amateurs, and small companies to get into the space industry due to their relatively low costs. Reducing the ground equipment and the system complexity supports the low-cost nature of these missions.

## 4.4 Ground Station Assumptions

When creating a ground-based tracking algorithm it is important to consider the positioning accuracy needs of the satellites which will be tracked. In order to support a mission that requires accuracy levels on the centimeter scale many factors must be taken into consideration. First, due to plate tectonics there is constant motion of the ground station. For example, stations on the North American plate will see movement to the southwest at approximately 2.3 centimeters per year. This figure differs in magnitude and direction depending on the specific plate, but regardless of location, there is always movement to consider. Fortunately, the rate of movement due to tectonic shifting is extremely small.

Another source of movement is the tidal shifts caused by the sun and the moon. The moon's tidal forces cause a cyclical shift of roughly 55 cm, while the sun induces a cyclical shift of around 15 cm. Additionally, since the cycles are not in sync, the exact shift at any given time can be anywhere within that range. Although much quicker than the tectonic shifts stated earlier, the tidal movements of the ground are also relatively slow compared to other sources of positioning error.

There are a multitude of other error sources dealing with movement of the ground station ranging from hydrological to atmospheric pressure differences, but they all induce very small errors, and unless there are extreme situations, move very slowly.

For this program, positioning accuracy is neither expected nor required to be at the centimeter level, and for that reason, the sources of error dealing with movements of the ground station have been neglected, or rather assumed to be zero.

If a cube satellite mission comes about that requires such accuracy, changes can be made to the program to include these motions in the dynamical models.

## **4.5 Station Scheduling**

Scheduling tracking and communication times for a specific satellite at one ground station is a trivial task, but if there are multiple satellites to track and communicate with all in orbit at the same time, the task gets more complex. With the number of missions currently worked on by the Texas Spacecraft Laboratory this will soon be a reality. The failure of the Antares launch vehicle in October of 2014 pushed back this deadline, but with multiple other missions underway the time is approaching quickly. As such, it is important that the ground station has a robust system for determining priority rankings for each satellite's communication time.

This section discusses the goals of a communication scheduling system and the challenges met in order to reach those goals. It discusses topics researched by others while also adding new areas of consideration.

### **4.5.1 Pass Strength Considerations**

When analyzing the strength of an overhead pass, the easiest figure to consider is the peak elevation of the pass. Other figures such as the duration of time that the satellite is overhead and the range from the station to the satellite are really products of the peak elevation. When considering many different orbit types and semi-major axes, the problem can become more complex. In the case of only LEO, nearly-circular orbits, the peak elevation is the key factor to be looked at. If a

satellite pass has a peak elevation of  $90^\circ$ , then it will pass directly over the ground station. This is the best case scenario, but is extremely rare. On the other extreme, a satellite with a peak elevation that is less than  $10^\circ$  will barely rise above the horizon, and often will not ever be picked up at a ground station. This is due to the amount of power lost due to the longer slant range, the misalignment of the transmitting antenna on the satellite, and even simple obstructions on the ground such as buildings and other structures.

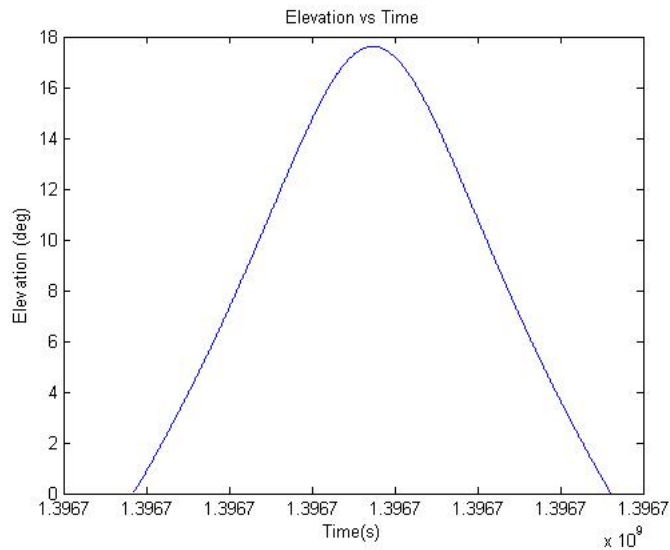


Figure 4.4: Elevation curve displaying a low-elevation pass. This satellite pass peaks at a low elevation which means that the slant range is long and the satellite is overhead for a shorter period of time. This is an example of a lower quality pass.

As the elevation increases, the slant range will decrease along with the alignment losses that come from the satellite pointing directly nadir at all times in the orbit. These characteristics lead to the most simplified potential ranking system by giving satellites that reach a higher elevation a higher tracking priority.

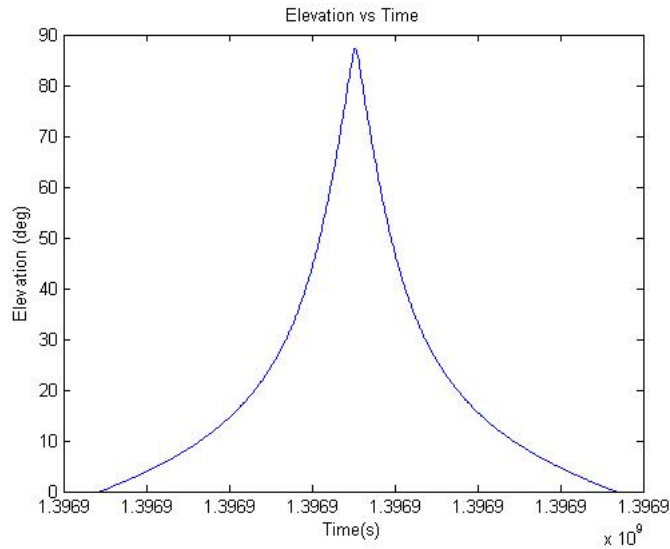


Figure 4.5: Elevation curve displaying a high-elevation pass. This pass peaks at a higher elevation meaning that it is more directly overhead and the slant range is smaller. This is an example of a higher quality pass.

#### 4.5.2 Management of Position Uncertainty

Position uncertainty over time is the main focus of the tracking fidelity analysis later in this thesis, but in the context of scheduling it is a topic worth briefly discussing. Using modern radars, studies have been done to show how position uncertainty grows over time for satellites that have not been tracked. In the case of a LEO satellite, operators can expect between one and four overhead passes over the course of one day, depending greatly on the shape and size of the orbit. Unfortunately, many of these passes may not be useable for tracking and normal communication due to the short period of time that they will be above the horizon and the extended slant-range of low-elevation passes. As time passes, the incurred error in the prediction propagation will continue to grow.



In order to ensure that operators do not lose custody of a satellite, periodic observations must be made so that new corrections can be made to the orbit. Then, a new set of predictions can be generated in order to keep the process moving as it would normally. The rise in uncertainty forces a corresponding rise in the tracking priority of that satellite. This changing weighting system could be added into the existing scheduling program to again shift operational priorities to meet mission necessities. In the worst case scenario, operators would lose custody over the satellite track and would need to potentially use external sources to reacquire the ability to accurately track the satellite.

#### **4.5.3 Management of Onboard Memory**

The data needs of cube satellite mission varies greatly in each case. For some missions engineers are focused on a small number of items or areas of interest and so the data is low volume and easily able to be downlinked over each pass. For other missions, onboard memory handles the excess data by storing it to then be downlinked at another time. However, for many missions, getting all the needed data from the satellite to the ground proves to be very difficult. For these missions, the data downlink needs can overrule other ranking systems.

In the case of high volume data a satellite can be given a weight to push it higher in the priority list when compared to normal ranking systems. This solution would allow operators to use any ranking system they choose, and add in a weighted score to skew the results slightly more in favor of the high data volume satellite. Further, it would allow the system to continue to operate in an automated fashion, removing the work from ground operators who may have other tasks to accomplish.

#### **4.5.4 High Priority Communications**

Beyond updating an orbit track, managing onboard memory levels, and using elevation rankings, there will be times when communicating with a specific satellite is a mission necessity. If the satellite is ailing or functioning in a non-ideal way, ground operators must track and command the satellite. These necessary commands to switch mission modes, diagnose an issue, downlink all stored data, or simply move into a power saving standby mode while engineers discuss a problem on the ground are extremely important, and thus supersede any other priorities during a specific pass.

During initial acquisition and start-up phases of the mission, the satellite will have priority for the ground station time. Once the mission has moved into a more automated, repeatable, and sustainable phase ground station priorities can shift back to normal ranking and scheduling systems. Finally, around the end of the mission lifetime, or near the time of re-entry, the priority ranking would be modified until the actual end of mission could be confirmed.

## Chapter 5

### Orbit Prediction and Tracking Algorithms

The main contribution of this research is the creation of two orbit modeling algorithms, both of which allow the user to predict overhead passes of any satellite for use with scheduling and mission planning. Further, the programs create detailed data products showing key characteristics of each pass so that operators can make educated decisions quickly or allow an automated system to handle the scheduling and communications. These two modes are composed of many fundamental building blocks as well as specifically derived algorithms catered to the problem of orbit prediction, correction, and updating.

This chapter discusses all facets of the two main operational modes for this tracking software and details the expected outputs at each stage in the process.

#### 5.1 Mode 1: Initial Orbit Prediction & Modeling

The first mode of operation for the program functions similarly to many other propagators taking a two-line element set input from an external source and using a  $J_2$  propagator to create a satellite ephemeris and pass predictions for the ground station. The main reason that this mode is not a stand-alone program is that there are problems with using TLEs alone to estimate orbital position. First of all, as time passes the errors within the integrator will increase in size. Secondly, the

initial TLE itself may not be extremely accurate, or even accurate enough to satisfy mission requirements for positioning knowledge. Finally, the continued maintenance of the estimated orbit relies wholly on the source of the TLE, which may not be suitable for cube satellite operators.

This section is composed of the goals, procedures, and results of mode one for the orbit tracking program. It discusses the capabilities and challenges of this method of orbit estimation and presents a way to integrate this method with other estimation methods.

### **5.1.1 Mode 1 Goal**

The primary goal of this mode of operation is to provide the ground station user with an initial nominal estimate of the orbit for the satellite of interest. By creating a useable, nominal estimate the batch mode differential correction algorithm of mode two will function effectively.

The point of contention for this mode of operation is errors may exist within the two-line element set for the specified satellite. These errors would propagate into the nominal estimate of the orbit path. Although this is a setback, this problem is not insurmountable. For this case, Doppler measurements will need to be taken for the first satellite pass. Then, the user would compare the curve provided by Doppler to the curves created by the propagator and temporally shift the estimation until the curves are most closely aligned. Then, at this point, a useable nominal state vector is drawn from the estimate to use as the nominal value for mode 2. At this point, normal operation of mode two would commence.

### 5.1.2 Procedures

The first procedure for this mode of operation is to select a recent two-line element set for the satellite of interest. It is important to select the most recent available TLE because as more time passes, the operator will need to propagate the state of the object further in time in order to get to a pass that will arrive in the near future. As the integrator moves in time, errors will accumulate, causing the expected passes to be inaccurate and possibly useless.

Next, the program will automatically read and process the TLE. Using the SGP4 algorithm, the state is then propagated for a single day. Finally, the data is prepared for post-processing. Apart from using SGP4, the operator could convert the TLE into an initial state vector. This initial state vector would then act as the start of the integration. Now using an integrator based on gravitational parameters and drag, the integrator automatically runs for the selected period of time. Again, twenty-four hours is far enough to find a useable pass for the typical low-earth orbit. However, longer periods of time can be used as long as the operator is willing to handle more potential errors. In this case, the operator would be using a set of mean elements in place of normal osculating elements for the propagation process. Using the SGP4 algorithm is the conventional method of inverting the original process used to convert the osculating elements found by observation into the mean elements of the set.

Upon completing the integration, the program immediately shifts into the post-processing. This post-processing includes converting the state vectors from an ECI frame to an ECEF frame. Next, the state vectors are then converted again

into the topocentric frames, which were the SEZ frame in the case of range and range-rate background calculations and the ENU frame for ground operations.

It is worth noting that the topocentric frame is located at the specific point on the Earth where the ground station antenna is located. This is important in order to ensure that the directions calculated for the antenna tracking are accurate. Finally, the topocentric position vectors, meaning the first three elements of the state vector which correspond to the position of the satellite, are converted into azimuth and elevation, the two angles which are defined as the angular offset from local north and the angle above the horizon. All of these different vectors serve a purpose in the visualization of the orbit, scheduling of the ground station, and logging for future reference if any analysis should require information as to the position or velocity of the orbit.

Now that the post processing has completed all calculations and logged all relevant information, the program begins the pass prediction portion of the code. An analysis of the elevation data selects all times at which the satellite is above the horizon and dumps the time spans along with all other state vector information into separate spreadsheets. The files are titled with the start time of the pass, and given headers to indicate summarized information about the pass. This information includes the total time of the pass, the total time above fifteen degrees elevation, the peak elevation, and several other ancillary items. These items are used to determine the strength of pass, which allows operators to see exactly which passes are of high value and which may barely become visible. In this program, the selection of passes to track is left at the discretion of the operator, but with the information provided in the pass files, an automated system could easily be created. In the case of one

satellite, the system would simply attempt to track each pass regardless of any poor characteristics. In the case of multiple satellites, a ranking system could be used. This would incorporate the strength of the satellite pass as well as the time since a satellite was last tracked.

This marks the conclusion of the first mode of operation. In normal operation, mode one would no longer be needed. If operators lose custody of the satellite using mode two, the first way to check current predictions would be to revert back to the TLE method.

### **5.1.3 Resulting Outputs**

For this mode of operation, there are a number of important outputs to consider in a ground station for use with tracking, scheduling, and communication. First of all, the estimated orbit ephemeris is created and placed into a backup master file for use if the ground station personnel need extra information. Secondly, the post-propagation analysis done through mode one creates files with the satellite track, denoted in azimuth and elevation, for each of the upcoming passes. Additionally, these files are given notes that rank each pass based on the strength of the pass to ease scheduling challenges in the case of multiple satellites moving overhead simultaneously. Next, the program creates a number of visualizations which help the users select a useful pass to track, understand the Doppler expectations for the specified pass, and analyze the secular motion of the satellite due to perturbations yielding larger changes over time. Finally, mode one delivers nominal state vector estimates for each pass so that when the user records Doppler data, it can be directly applied through mode two in order to update the satellite ephemeris estimate.

A unique challenge can potentially arise when using the topocentric angle tracks as inputs to an antenna rotor controller. Satellites orbiting the Earth in nearly circular, low orbits move quickly across the sky. In cases where the peak elevation is no higher than around  $70^\circ$  there is no issue, and the antennas can smoothly follow the track of the satellite. In cases where the satellite's track crosses or comes close to the zenith point, the controlling rotors may have trouble keeping up with the motion. This is a major problem for low-cost rotors and rotor controllers, as it risks the loss of valuable communication and tracking time.

In order to combat this problem, a solution, dubbed the "keyhole problem" was developed. When the satellite track moves past an elevation limit, potentially around  $80^\circ$ - $85^\circ$ , the rotor ceases all motion upward in elevation and instead, slews the azimuth control to the point where the satellite will be in the sky when it comes back down to the elevation limit set earlier. Then, the controller proceeds to follow the satellite track as it would normally.

Every satellite pass is slightly different and every ground station contains different equipment. As such, the details on what elevation limit is best for a single pass is unique to that pass. An example is given in Figures 5.1.1 and 5.1.2.

Additionally, it is worth noting that a hard elevation limit is not always the best solution. Using curved tracks where the elevation controller continues to rotate in order to meet back up with the satellite quicker can marginally increase communication time. However, they increase the system complexity and require additional effort to implement on every chosen pass.



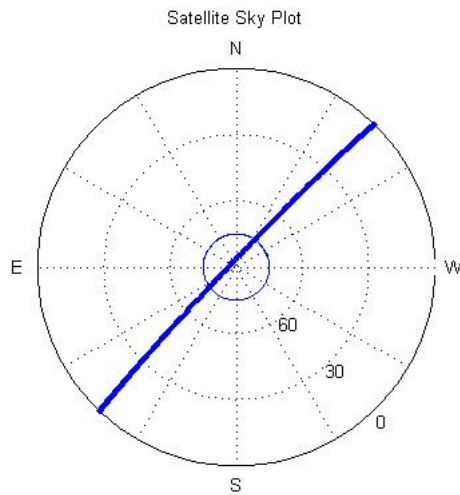


Figure 5.1: Satellite track passing above the 80° limit.

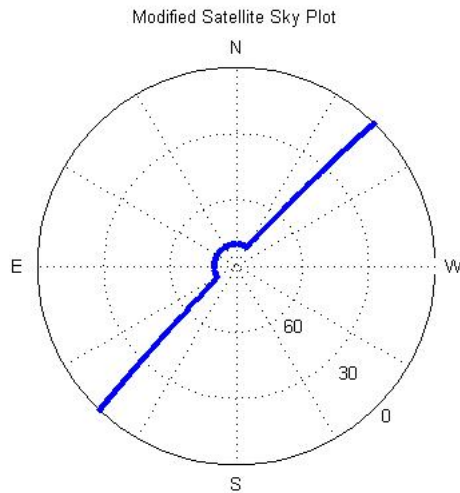


Figure 5.2: A modified satellite track created to ensure the rotors keep pace with the satellite's motion.

#### 5.1.4 Two-Line Element Sets

A two-line element set is a brief, but thorough, description of a satellite's orbit characteristics at a specific epoch. The entire set consists of two lines, each

with only sixty-nine characters. The lines are numbered at the beginning as can be seen below.

```
1 25544U 98067A 15044.29415176 .00024437 00000-0 36701-3 0 9999
2 25544 51.6480 342.7631 0005921 3.1886 156.4383 15.54724594928752
```

Figure 5.3: Two-Line Element Set[21].

After the line indicator, in the first line the satellite identifier is given along with a classification and international designators. After these elements, the epoch is given. For the above figure the epoch can be interpreted as 44.29415176 days into the year 2015. Next in the first line there are derivatives of the mean motion, a modified drag term, more classification numbers, and a checksum.

The bulk of the elements that describe the orbital motion are contained in the second line. As in the first, the line number and satellite number are given. After that however, the inclination, right ascension of the ascending node, eccentricity, argument of perigee, mean anomaly, and mean motion are given. Finally, a revolution number is given along with a final checksum.

These elements provide a succinct definition of a satellite's orbit at a specific epoch, and further, endeavor to provide information regarding the drag characteristics, lifespan, and history of the given object.

## 5.2 Mode 2: Continuous Orbit Model Update

The second mode of operation contains the main the method of estimating and propagating the true orbit of the satellite of interest. The algorithm utilizes information derived from mode one in combination with external measurements of

the frequency Doppler shift, conducted by the ground station operators during any overhead pass. With information on a nominal state vector, the batch estimation procedure will accurately estimate the orbit, proceed with orbit propagation, and then continue providing pass predictions and ephemerides in order to repeat the process. Once the system has entered mode two, there is no need to enter mode one again.

This section details the goals, procedures, and results of mode two. Additionally, it discusses key strengths of the method for use with cube satellite projects within the academic and scientific community.

### **5.2.1 Mode 2 Goal**

The primary goal of mode two is to provide ground station operators with an accurately estimated satellite ephemeris for any target satellite without the use of GPS or any other tracking technology. Additionally, this mode aims to quickly capture information from an overhead pass and apply it not only to check the validity of the current orbit track, but also to update the track to continually maintain the required levels of accuracy. Finally, mode two endeavors to supply operators with the foundation for a community system continually updating any satellite's orbital ephemeris via use of Doppler information. This scalability allows for many ground stations to work together in a simple way for the benefit of all and greatly increases the number of passes per day, which is especially important for LEO satellites.

## 5.2.2 Procedures

The first step in this mode is quite similar to the first mode of operation; the program will ask for a TLE to be input and read into the system. However, in the first mode, this TLE will be used only as a reference for ancillary information needed later in the algorithm.

After reading in the reference TLE, used to assign labels to the resulting data, the operator must select a spreadsheet file containing the measured frequency shift data. This data comes from direct observation of the satellite communication signal. It is very important that the time tags for each measurement are accurate so that the program can properly work through the differential correction process later. The final file to be loaded during the first phase of mode two is the specific prediction file created in mode one. This prediction file contains state vectors for each time instance along with Doppler predictions. This is the second major component needed for the differential correction process to proceed.

One caveat to this process is that the predicted file times may not perfectly align with the observed time. The predictions should be close, but almost never exactly correct. This is due to errors in the propagation and the original orbit characterization. The method used to get around this is to align the Doppler curves by syncing the zero crossings of the two data sets. Once this is done, the prediction file times are overwritten to match the observed times. Finally, the state vector that marks the beginning time for the predictions is selected as the initial nominal state vector. From here, the differential process can begin.

For the differential correction process, a batch mode least-squares estimator

was built and implemented. The estimation of the ECI state vector of the satellite at the selected epoch completes roughly three iterations before converging and proceeding with the next step in the process.

Once the batch mode processing has completed, the numerical integration commences. Now, the equations of motion are integrated for a full day in order to give ample time for the satellite to pass overhead. The integrator here uses the Keplerian forces along with the  $J_2$  gravitational parameter. If there was a need for higher accuracy in other missions then more parameters could be taken into account.

Finally, once the integration is completed, the state vectors are logged and the post-processing begins. From here, the program operates identically to mode one by converting the state vectors into the topocentric frames, calculating the azimuth and elevation angles, and creating pass prediction files. Once the process is complete, the pass prediction tables will serve as the new ephemerides. At this point, the method of determining the satellite's orbit uses tables of predicted data with an integration scheme. The system of using mean element sets is ignored in place of this bulkier, yet more precise methodology. Ideally, once the operator starts to use mode two, there is no reason to return to mode one. Mode two should be run continuously on each significant pass to keep a solid estimation of the current position and orbit.

### **5.2.3 Resulting Outputs**

There are a number of important outputs for mode two. The first of which is a backup ephemeris file which contains all state vector information over the new propagation time. As in mode one, the post-propagation analysis creates an orbit

track file for each satellite pass, detailing the direction of the satellite in azimuth and elevation. This allows for continued usage and maintenance of the orbit. Each pass is labeled with a priority rating, as in mode one, for scheduling purposes. Finally, the TLE information retained by the system is purely for backup purposes, but can be useful if the track is lost for some reason and mode one is needed. This could also be used by operators of different ground stations to help supplement the coverage of a specific satellite, or even continue communications with the satellite if a time-sensitive situation arises.

As in the mode one results, a special case exists for the antenna tracks called the “keyhole problem.” Operators must remember to incorporate the solution to that challenge into their controller inputs for any passes that pose a problem.

#### **5.2.4 Slant-Range Rate Derivation**

The estimation algorithm employed in mode two is built on understanding the Doppler shifts observed in the received signal. These frequency shifts are a product of the slant-range rate of the satellite when observed from the ground station. As such, it is important to understand the relationship between the satellite’s transmitted frequency, the frequency received at the ground station, and the slant-range rate of the satellite.

In order to calculate the slant-range rate for a satellite broadcasting at a specific frequency, consider the signal received at a ground station receiver of frequency  $f_R$  compared to the satellite’s original transmit frequency  $f_T$ . Defining  $\vartheta$  to be the angle between the range vector and the relative velocity vector, consider the following formula.

$$f_R = f_T \gamma (1 - \beta \cos(\theta)) \quad (5.2.1)$$

$$\beta = \frac{\vec{v}_{Rel}}{c} = \frac{\|\vec{v}_T - \vec{v}_R\|}{c} \quad (5.2.2)$$

$$\gamma = \frac{1}{\sqrt{1 - \beta^2}}$$

Next, the following manipulations are done to create a simplified expression.

$$\beta \cos(\theta) = \frac{v_{Rel}}{c} \frac{\vec{v}_{Rel} \vec{\rho}}{\|\vec{v}_{Rel}\| \|\vec{\rho}\|} = \frac{\dot{\rho}}{c} \quad (5.2.3)$$

Finally, one can assume that the relative velocity associated with the system is significantly smaller than the speed of light. This assumption leads to the value  $\gamma \approx 1$  which further simplifies the expression and yields the final formula for the slant-range rate observed at a specific set of frequencies.

$$f_R \approx f_T \left( 1 - \frac{\dot{\rho}}{c} \right) \quad (5.2.4)$$

$$\dot{\rho} = c \left( \frac{f_T - f_R}{f_T} \right) \quad (5.2.5)$$

### 5.2.5 General Batch Estimation Algorithm

The general batch estimation algorithm is an iterative process which begins with an initialization phase.

$$\begin{aligned}
i &= 1 \\
t_{i-1} &= t_0 \\
X^*(t_{i-1}) &= X_0^*
\end{aligned} \tag{5.2.6}$$

$$\Phi(t_{i-1}, t_0) = \Phi(t_0, t_0) = I$$

The next initialization portion depends on whether there is an a priori estimate. If there is an a priori estimate then the first row formulas are used. Otherwise, the values are set equal to zero.

$$\begin{aligned}
\Lambda &= \bar{P}_0^{-1} & N &= \bar{P}_0^{-1} \bar{x}_0 \\
\Lambda &= 0 & N &= 0
\end{aligned} \tag{5.2.7}$$

At this point, observation data is read into the program. Using this data, the reference trajectory and state transition matrix is integrated from  $t_{i-1}$  to  $t_i$ .

$$\dot{X}^* = F(X^*(t), t) \tag{5.2.8}$$

$$\dot{\Phi}(t, t_0) = A(t) \Phi(t, t_0) \tag{5.2.9}$$

$$A(t) = \left[ \frac{\delta F(X, t)}{\delta X} \right]^*$$

Now, the results of the current observation are accumulated using the following formulas.



$$\begin{aligned}
\tilde{H}_i &= \left[ \frac{\delta G(X,t)}{\delta X} \right]^* \\
y_i &= Y_i - G(X_i^*, t_i) \\
H_i &= \tilde{H}_i \Phi(t_i, t_0) \\
\Lambda &= \Lambda + H_i^T W_i^{-1} H_i \\
N &= N + H_i^T W_i^{-1} y_i
\end{aligned} \tag{5.2.10}$$

Next, this phase continues by updating each component.

$$\begin{aligned}
i &= i + 1 \\
t_{i-1} &= t_i \\
X^*(t_{i-1}) &= X^*(t_i) \\
\Phi(t_{i-1}, t_0) &= \Phi(t_i, t_0)
\end{aligned} \tag{5.2.11}$$

If all observations have been processed, then the algorithm moves on to the next step. Otherwise, the reading of data, integration, accumulation, and updating process repeats.

Once the data has been completely accumulated and processed, the normal equations are solved along with the covariance.

$$\begin{aligned}
\hat{x}_0 &= \Lambda^{-1} N \\
P_0 &= \Lambda^{-1}
\end{aligned} \tag{5.2.12}$$

The iteration is completed when the nominal trajectory is updated.

$$X_0^* = X_0^* + \hat{x}_0 \tag{5.2.13}$$

If the solution has converged, then the process is complete and the estimation algorithm stops. However, if at this point the solution has not converged then  $\bar{x}_0$  is shifted with respect to the new nominal by doing  $\bar{x}_0 = \bar{x}_0 - \hat{x}_0$ , and the process iterates.

### 5.2.6 Slant-Range Rate Batch Estimation Implementation

The slant range rate batch estimation implementation uses the general algorithm presented in the prior section of this thesis, but with specific equations relating to the problem of interest. The first major component of the algorithm is the selection of the state vector. This state vector contains each variable to be estimated.

$$X = \begin{bmatrix} x \\ y \\ z \\ \dot{x} \\ \dot{y} \\ \dot{z} \end{bmatrix} \quad (5.2.14)$$

Next, consider the dynamical model used in the differential process. For this application, the two-body model was supplemented with the perturbation due to  $J_2$ , yielding the following expression of the potential.

$$U = \frac{\mu}{r} - \frac{\mu}{r} \left(\frac{R}{r}\right)^2 J_2 \left(\frac{3}{2} \left(\frac{z}{r}\right)^2 - \frac{1}{2}\right) \quad (5.2.15)$$

$$r = \sqrt{x^2 + y^2 + z^2}$$

At this point, the partial differentials of the potential function were taken in order to produce the linearized form of the equations of motion.

$$F = \begin{bmatrix} \dot{x} \\ \dot{y} \\ \dot{z} \\ \frac{dU}{dx} \\ \frac{dU}{dy} \\ \frac{dU}{dz} \end{bmatrix} \quad (5.2.16)$$

Now, introduce the state transition matrix and recall the following formula relating the state transition matrix to its derivative. Define A in the following way.

$$\begin{aligned} \dot{\Phi} &= A\Phi \\ A &= \frac{dF}{dX} \end{aligned} \quad (5.2.17)$$

In order to properly utilize this model, one must remember that thus far the calculations have been done in the ECI frame, but the station coordinates are stated in the ECEF frame. In order to proceed, a rotation is done using the inverse of equation 3.2.22 and along with equation 3.2.23 in order to convert the station coordinates from ECEF to ECI.

The next important section deals with the model of the observations. In many cases the slant-range formula is used, but in this case the slant-range rate is required. Stating the range expression, the partials are then taken in order to reveal the proper observation model, G.

$$\vec{\rho} = \begin{bmatrix} (x - x_s) \\ (y - y_s) \\ (z - z_s) \end{bmatrix} \quad (5.2.18)$$

$$\rho = \sqrt{(x - x_s)^2 + (y - y_s)^2 + (z - z_s)^2}$$

$$\dot{\rho} = \frac{d\rho}{d\vec{r}} = G = \frac{[(x-x_s)v_x + (y-y_s)v_y + (z-z_s)v_z]}{\sqrt{(x-x_s)^2 + (y-y_s)^2 + (z-z_s)^2}} \quad (5.2.19)$$

Finally, derive the matrix which describes the sensitivities of the observation model to each estimated element. The expression used to derive the matrix is seen below, followed by the results.

$$\tilde{H}_i = \left[ \frac{\delta G(X, t)}{\delta X} \right]^* \quad (5.2.20)$$

$$\tilde{H}_i = \begin{bmatrix} \frac{v_x}{\sqrt{(x-x_s)^2 + (y-y_s)^2 + (z-z_s)^2}} - \frac{2(x-x_s)(v_x(x-x_s) + v_y(y-y_s) + v_z(z-z_s))}{(2((x-x_s)^2 + (y-y_s)^2 + (z-z_s)^2))^{\frac{3}{2}}} \\ \frac{v_y}{\sqrt{(x-x_s)^2 + (y-y_s)^2 + (z-z_s)^2}} - \frac{2(y-y_s)(v_x(x-x_s) + v_y(y-y_s) + v_z(z-z_s))}{(2((x-x_s)^2 + (y-y_s)^2 + (z-z_s)^2))^{\frac{3}{2}}} \\ \frac{v_z}{\sqrt{(x-x_s)^2 + (y-y_s)^2 + (z-z_s)^2}} - \frac{2(z-z_s)(v_x(x-x_s) + v_y(y-y_s) + v_z(z-z_s))}{(2((x-x_s)^2 + (y-y_s)^2 + (z-z_s)^2))^{\frac{3}{2}}} \\ \frac{(x-x_s)}{\sqrt{(x-x_s)^2 + (y-y_s)^2 + (z-z_s)^2}} \\ \frac{(y-y_s)}{\sqrt{(x-x_s)^2 + (y-y_s)^2 + (z-z_s)^2}} \\ \frac{(z-z_s)}{\sqrt{(x-x_s)^2 + (y-y_s)^2 + (z-z_s)^2}} \end{bmatrix}^T \quad (5.2.21)$$

This matrix is useful in many ways, such as inspecting the dependencies and looking for redundancies in the estimation. By inserting these derived expressions into the general algorithm previously explained, one can commence with the estimation process.

## **Chapter 6**

### **Prediction Fidelity Analysis**

Low-cost cube satellites are placed into orbits that are convenient for the launch system, whether that be a rocket or from the International Space Station. As such, they are most commonly placed in low-Earth orbit where they can orbit for a few years before re-entering and burning up. This policy is convenient for managing space debris in LEO, but also poses a challenge for mission operators. In LEO, the success of a mission depends largely on the number of passes that are useful for communication in a certain amount of time. Also, for tracking purposes it is important to supplement predictions with real observations. Thus, it is important to understand the number of passes that are expected for each satellite, and the level of error in predictions that should be expected for relevant software.

This chapter looks at the frequency that a satellite will pass over a certain ground station depending on the orbital inclination. Secondly, it discusses the error sources of numerical integrations of satellite orbits. Finally, it combines the results of each analysis in order to deliver an error prediction analysis of different satellites.

#### **6.1 Pass Frequency Investigation**

Understanding the relative geometry between an orbiting satellite and a fixed ground station is important in order to be able to assess the usefulness of a

specific station. The key elements of the problem are the ground station's latitude and the satellite's orbital inclination. The inclination of the orbit will dictate what latitude the satellite will reach. If a satellite in a 400 km, near-circular orbit moves around the Earth with an inclination of  $10^\circ$ , then a ground station at  $35^\circ$  will never see it. For this investigation the position of the Texas Spacecraft Laboratory ground station is used, although the same analysis could be applied to any station, or further, a network of stations. The most important factor in this analysis is the latitude, and for the laboratory the latitude is roughly  $30.29^\circ$ .

### **6.1.1 Inclination-Based**

Doing a simple numerical integration of 400km, near-circular orbits with inclinations from  $10^\circ$  to  $80^\circ$  reveals the common "shark-fin" pattern. This shows the total number of overhead passes for any inclination at the specified orbit. Examining the data it is clear that for this ground station, the satellite's with inclinations between  $30^\circ$  and  $50^\circ$  will pass overhead the most, but there is no comment on the strength of each pass.

Looking further at the data, one can see the time between each satellite pass, and noticeable patterns emerge. First, there is a phase in the precession of the orbit in which the satellite will pass by the station on consecutive revolutions, yielding the bottom line of data. It is important to note that this area represents a small amount of time in the satellite's relative motion around the Earth. Beyond that phase, the relative geometry negatively affects the frequency of the passes. For inclinations lower than the station, the cyclic nature causes long droughts where no passes come overhead. This trend shifts lower in time as the inclination increases.

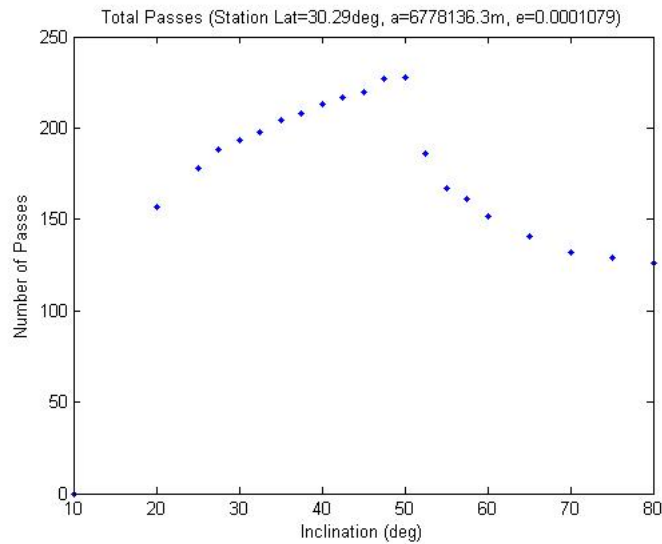


Figure 6.1: “Shark-fin” style graph showing total passes over a 30 day span.

Once the satellite’s inclination has moved significantly above the station’s latitude, there exists numerous different phases with staggered times. Finally, moving further upward in inclination again increases the time between passes overall.

### 6.1.2 Pass Strength Inclusion

Unfortunately, the purely inclination-based study does not reveal the true nature of the data. In order to fully assess how often a satellite will pass overhead to be communicated and tracked, one must also look at the quality of the passes being recorded. This is done here by examining the peak elevation of each pass. The peak elevation provides a good metric in this controlled scenario because, when dealing with mainly circular orbits at LEO, a larger peak elevation will indicate a smaller slant-range, less angular misalignment in the antennas, and a generally longer pass. Examining passes over 30° first yields the information in Figures 6.1.3 and 6.1.4.

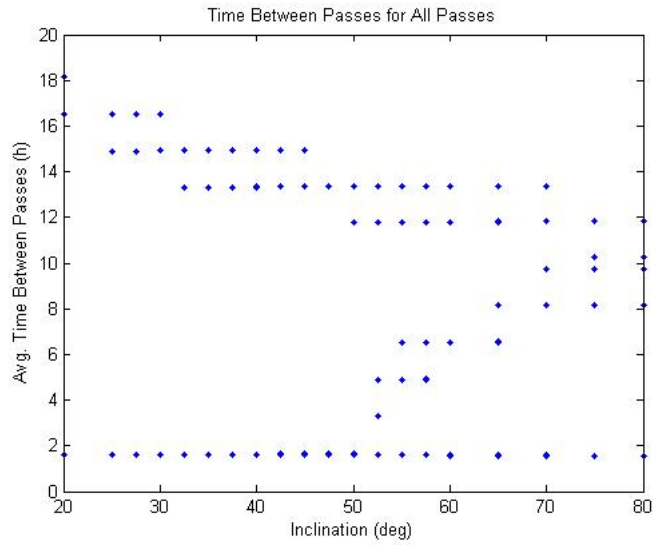


Figure 6.2: Time between each satellite pass over a 30 day span.

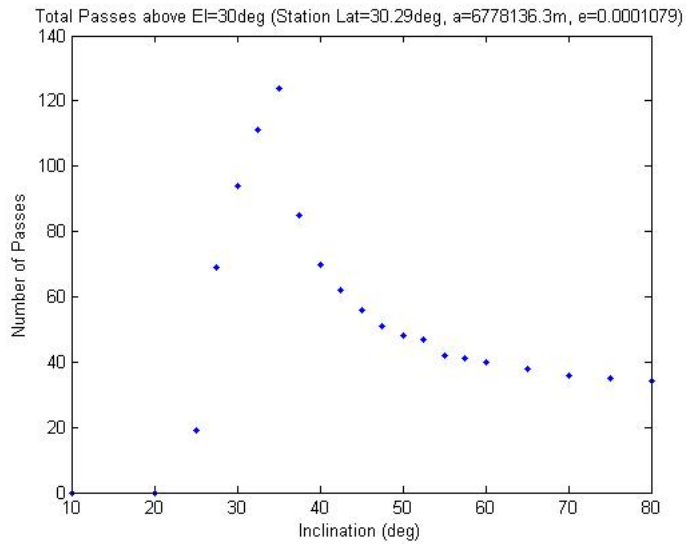


Figure 6.3: Total satellite passes reaching above 30° elevation over a 30 day span.

Already a large difference can be seen in the data. At the 30° elevation the station should be able to communicate for a short period of time. Below this figure,



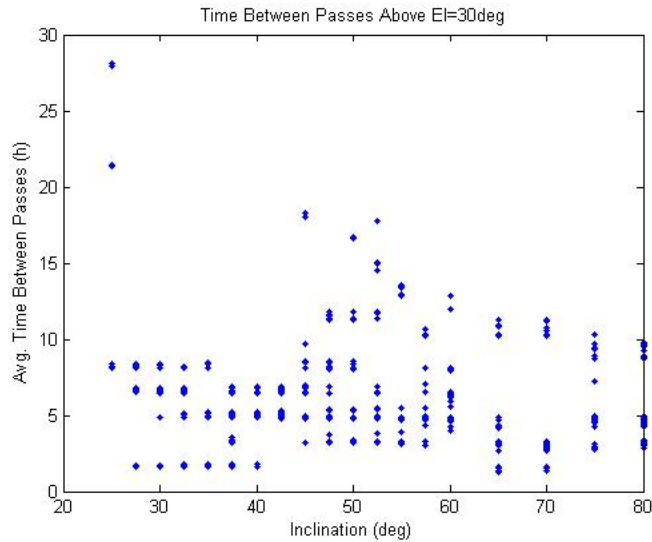


Figure 6.4: Time between each pass above 30° elevation during a 30 day span.

communication will be more difficult, and thus, the passes in that area will be less important. In the overall pass data, the “shark fin” pattern is exaggerated, while the total numbers of passes are significantly reduced. Looking at the time data, the area with the most consistent passes is shown to be just below the station latitude and up to roughly 10° above the station latitude. Other sections of data show numerous time intervals exceeding 8-10 hours. Narrowing the scope of the data, looking at strong passes above 50° yields the results in Figures 6.1.5 and 6.1.6.

Although the pattern in the overall number of passes remains, the timing data is less conducive to an obvious conclusion. Finally, narrowing the statistical data further to only those passes that peaked above 70° elevation yields the following results. The passes considered here would be very strong candidates from communication and tracking, but are also the rarest.

Examining the timing data shows some consistency within the inclinations

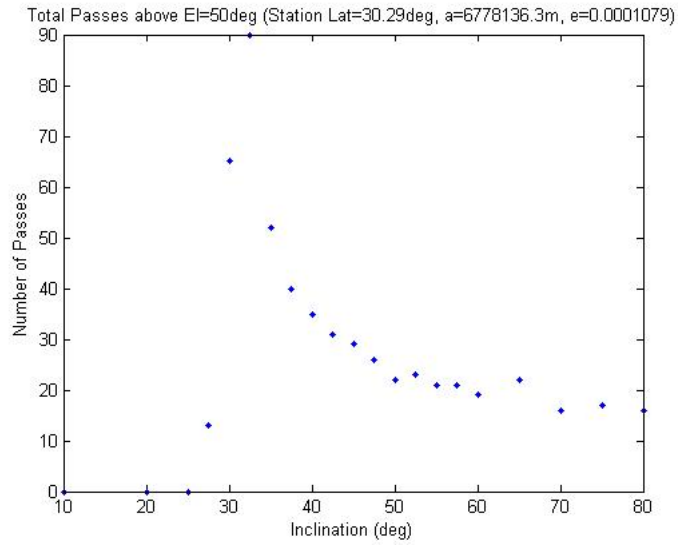


Figure 6.5: Total satellite passes reaching above 50° elevation over a 30 day span.

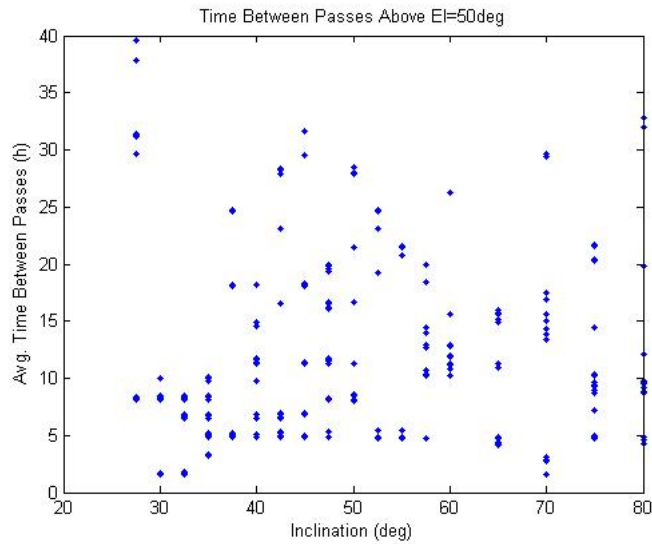


Figure 6.6: Time between each pass above 50° elevation during a 30 day span.

around and slightly above the station’s latitude, although the timespans overall are much longer. The lack of long, high-elevation passes for a satellite orbiting at LEO

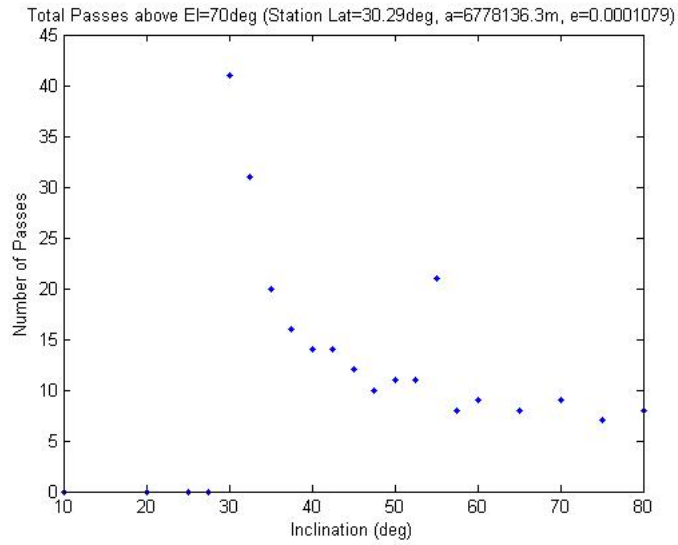


Figure 6.7: Total satellite passes reaching above 70° elevation over a 30 day span.

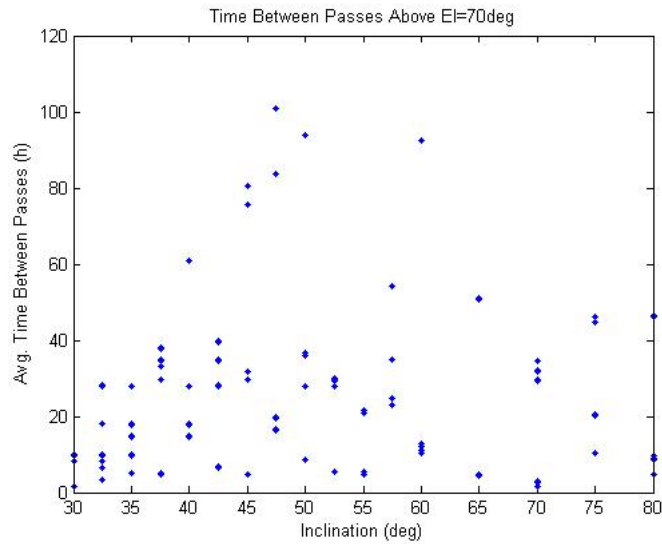


Figure 6.8: Time between each pass above 70° elevation during a 30 day span.

is a significant weakness for a single ground station to consider. With less common useable passes, the time between observations increases. This shifts the reliance of

operators from purely observations to numerical integrators and propagation techniques.

## **6.2 Prediction Error Sources and Rates**

In order to continuously monitor a satellite orbit and predict observable passes, operators must make use of orbit propagation techniques. These techniques were discussed earlier in this thesis, but now the errors involved in the process will be considered. There are a number of error sources to manage within any scheme, but for this investigation a  $J_2$  propagation scheme was used.

### **6.2.1 Dynamical Model Errors**

The predominating source of error within the  $J_2$  propagator comes from the differences of the dynamical model versus the actual environment. Within this category, there are a number of areas to consider. The first to look at is the ever-changing atmosphere of the Earth. Solar activity and the daily solar cycle of the Earth drive changes in the atmosphere which produce changes in the drag felt by the satellite. Major efforts to model drag using empirical data have been undertaken throughout the space age, but results are still very mixed. Overall, drag can and will produce large errors in the predictions. Beyond drag, there are a number of other sources of error to consider. The oblate nature of the Earth is accounted for in large part by the  $J_2$  term included in the model, but there are many other non-spherical properties of the Earth.

Also included in Figure 6.2.1 are some third-body effects. The other major

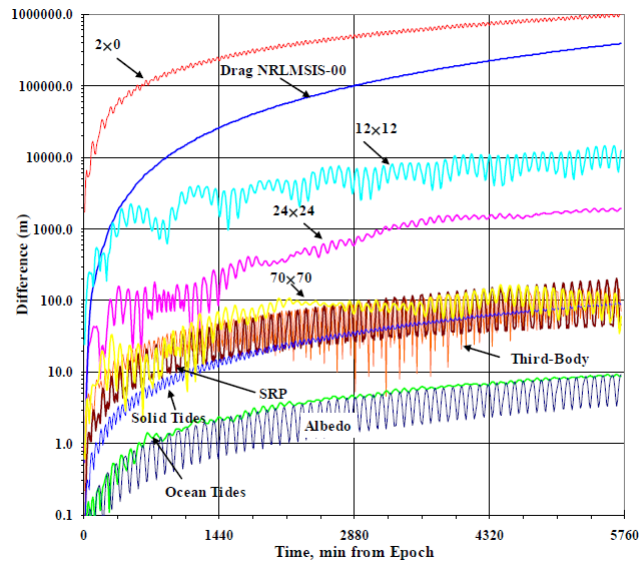


Figure 6.9: Graph depicting position differences over time for different models. Gravity models are compared to the next most significant[1].

bodies in the solar system produce perturbations that are ultimately very small, but still felt by the satellite. Hill's equations can be used in most cases based upon the assumption that the relative perturbation between the satellite and the primary is extremely small. For this reason, and due to the shorter time spans of integration, these forces were not considered.

### 6.2.2 Integrator Error

Another source of error relies on the numerical integrator rather than the dynamical model. No matter what integrator the operator chooses to use, the numerical solution will not be perfectly exact. The numerical solution attempts to be as close as possible to the unattainable symbolic solution.

Many integrators use variable steps in order to manage the truncation error

and subtraction error, keeping the total error from any particular sub-interval within a specific tolerance. Over time, the error from each sub-interval will accumulate. One method of reducing the incurred error over time is to use a higher order integrator, although this solution is not always recommended. Increased accuracy will come at the cost of more function evaluations requiring more computing time[4].

In order to reduce the overall error from the integration, operators must choose to track any and every observable pass that arrives so observations can be used to correct the orbit and reset the error accumulation. This is not a difficult choice for users, as the success of the mission depends on communicating with the satellite as often as possible.

For this application the Matlab ode45 function was used. Within the framework of the Matlab function there are a number of error tolerances which can be programmed into the system. In order to proceed with the integration the program must execute each step while satisfying the error tolerances. Picking a larger tolerance allows the program to execute more quickly, while a more strict tolerance would require more function evaluations and subsequently take more time[26]. In order to keep errors low, the tolerances were set at  $1 \times 10^{-10}$ .

### **6.3 Expanded Network Potential**

The analysis done here considered a single ground station, and it is clear that an expanded network would yield much better statistical results. Constructing another station at a different latitude would allow for better varying coverage of different inclination orbits, while a station at a different longitude could significantly

reduce the time between useable passes. These facts strongly support the potential for cooperative efforts between universities, amateur groups, and private industry to further the communication and tracking capabilities in the cube satellite domain.

There is a potential for future work in which engineers would place additional ground stations at different locations and run the same study to determine the most efficient geographical layout.

## **Chapter 7**

### **Tracking Analysis and Results**

The orbit modeling and pass prediction algorithms presented here are important to the tracking and scheduling process. In this tracking program there are two main modes of operation; the first relies upon TLE sets while the second takes a priori information and updates it using Doppler observations. By using both of these mechanisms, ground station operators can maintain an orbit model with current predictions without the use of GPS or any external information sources.

This chapter focuses on the results of each portion of the tracking algorithms. Further, it attempts to quantify the results of each model and prediction.

#### **7.1 Mode 1 Testing and Results**

Mode one testing will be focused on the ability of the algorithm to interpret TLE information, establish all initial parameters, propagate the orbit, process each data point, and produce output prediction files. The results will be explained additionally with multiple visualizations.

##### **7.1.1 Test Case Selection**

The original purpose of this research was in support of the RACE mission, so the simulated test case uses the orbit of the International Space Station. For this



portion of the test, a TLE was selected as the basis for the mode one propagation and prediction. Interpreting the TLE yielded the following initial orbit element values and state vector as reported by the program itself during operation.

```

Initial Orbital Elements
Semi-Major Axis [m] : 6781247.737766
Eccentricity [] : 0.000308
Inclination [deg] : 51.652100
Argument of Perigee [deg] : 347.052300
RAAN [deg] : 104.421500
True Anomaly [deg] : 51.652100

Initial State Vector
Rx [m] : -893650.182621
Ry [m] : -6022682.900132
Rz [m] : 2990049.459477
Vx [m/s] : 4882.023410
Vy [m/s] : -3193.439489
Vz [m/s] : -4971.305235

```

Figure 7.1: Initial propagation parameters reported by the mode one program execution in Matlab. These parameters correspond specifically to the ISS.

These values align with the expected results for the chosen TLE and are used by the propagator to predict the orbit trajectory over the next day. Additionally, the initial epoch information and relevant tagging parameters are recorded, but not reported at the start of the program. This information is later produced in the pass prediction reports.

### 7.1.2 Orbit Prediction Results

The first mode of operation primarily deals with the initial reading of information and the propagation which gives operators pass predictions for the following day. As such, the figures display the results of that propagation.

There are additional plots of the spacecraft's velocity, orbital elements, az-

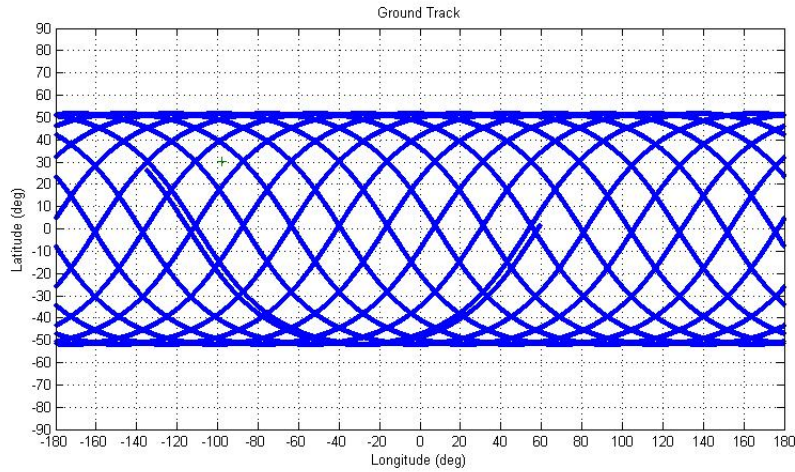


Figure 7.2: Ground track of the resulting 24-hour propagation displays the two-dimensional trajectory of the spacecraft overlaying the Earth.

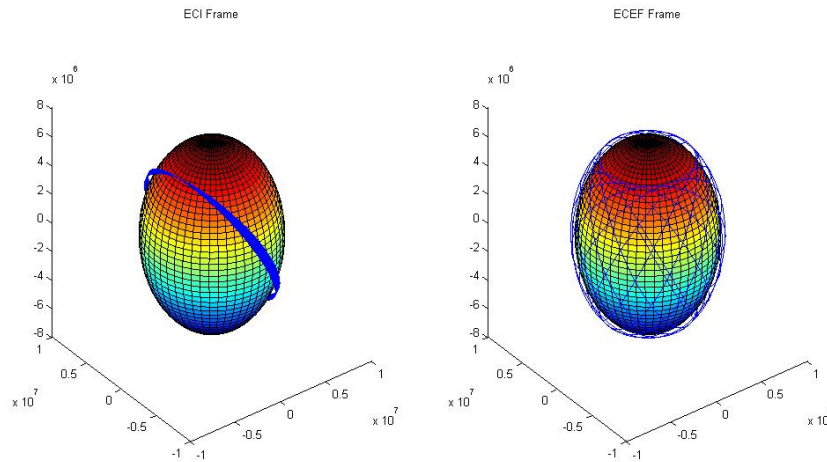


Figure 7.3: Three-dimensional plots of the spacecraft's trajectory seen in two different frames.

imuth, and elevation over time that can be used as reference by the operators, but what is important is the report generation that occurs at the end of the program. For this specific propagation, there were six passes recorded with varying strengths.

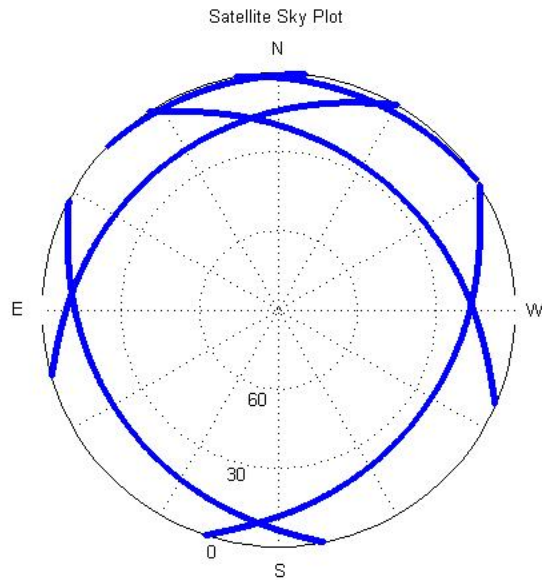


Figure 7.4: Skyplot displaying each of the six overhead predicted passes.

According to the data, there will not be a single pass above thirty degrees elevation. This is not preferable, but is still workable for the program. In the case of real tracking, the operators would choose as many passes as possible for communication and observation. For the case of this testing, one pass will be selected.

The speed of the code run here is not an important factor in the overall design of mode one and so it has not been analyzed. Code was created in Matlab for experimentation and would be converted to another language for full implementation, but regardless, the function of mode one is not to run in a time-sensitive environment, but rather to provide initial data points.

## **7.2 Pass Selection and Observation**

For testing, it is important to select a pass that is potentially useable and to see how the process proceeds through the differential correction process. In this section, a pass is selected and observed data is simulated in order to provide a more realistic baseline for the orbit and also provide Doppler predictions. The predicted data is modified to incorporate potential noise of the system.

### **7.2.1 Manual Pass Selection**

In this case, the pass selected for processing had a peak elevation of roughly 26°. In most cases this pass would not be preferable for use with the program, but unfortunately the passes found in the previous day were not of high elevations. This limits the capabilities of the differential correction process, but is a common challenge met by operators dealing with low-Earth orbiting satellites. The elevation curve is shown below in order to display the characteristics of the pass. Additionally, a sky plot was created in order to further visualize the pass.

### **7.2.2 Simulated Observation Data**

For this testing, the Doppler curve produced by the prediction software is assigned to be the true nominal state of the satellite. In order to create a set of data more akin to actual observations, a new set is created by combining the true nominal data with a set of random Gaussian noise. Further, the total data is trimmed to simulate receiving communications a short time after the satellite has appeared above the horizon. Using a nadir-facing communications system, it is unlikely that a signal will be received immediately as the satellite begins passing above the horizon.

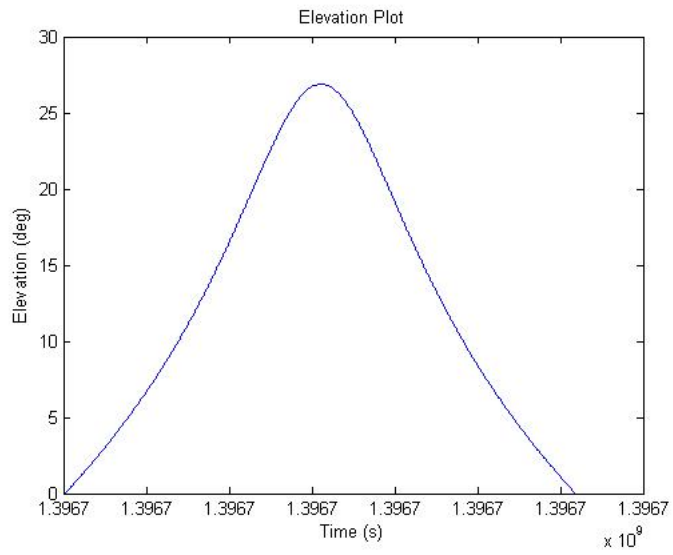


Figure 7.5: Plot of the elevation versus time for the pass selected for processing.

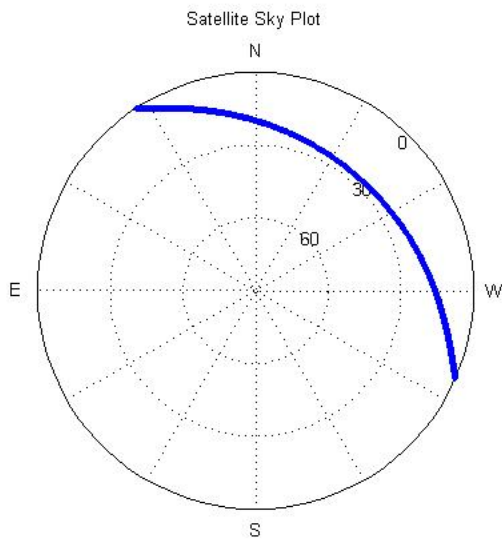


Figure 7.6: Sky plot of the pass selected for processing.

A section of the true nominal is displayed below along with an observation signal in order to visualize the added noise.

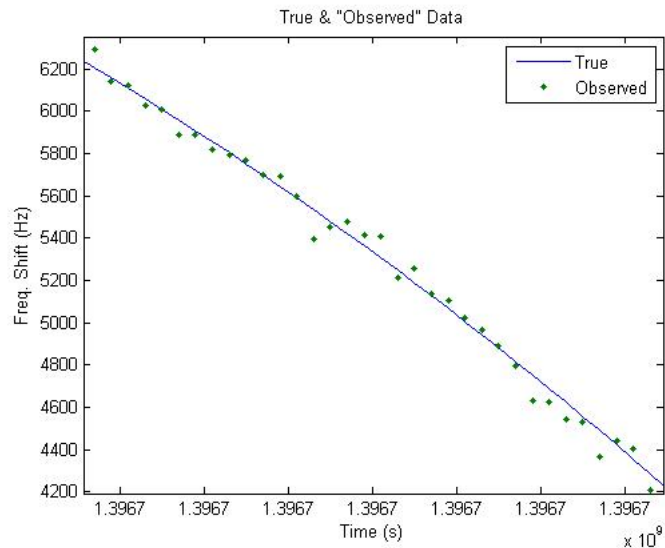


Figure 7.7: A portion of the true Doppler shift curve and simulated observations with added Gaussian noise.

Lastly, an important note for this testing is that the Doppler curves provided here are both continuous. In actuality the signal may not be as perfectly continuous. Further, if the operators use a beacon signal, the data will be extremely discontinuous, but the resulting curve should be of a similar nature. In that case, a low elevation pass may be unusable.

### 7.3 Mode 2 Testing and Results

The testing of mode two focuses on the applied procedures, initial nominal state selection, correction process, and resulting outputs. There are manual operations in addition to the automated processes within the algorithm, and they are

explained in detail for future reference. Particular emphasis has been put on the ability of the algorithm to continuously update and monitor a particular orbit.

### **7.3.1 Time Matching**

A key factor in aligning the observations with the correct predictions is matching the time precisely. By using numerical integration to predict the values a misalignment will accrue over time. This misalignment is small, but significant when looking to correctly predict the satellite's location and orbit. The method proposed here exploits a common characteristic of this type of Doppler curve.

The method involves matching the zero-crossing point in the two Doppler curves. Recalling the characteristics of a circular orbiter at LEO's Doppler curve, there will be a point at which the Doppler shift is exactly zero. This point corresponds to the time when the satellite is at its peak elevation. By aligning the two points, operators are able to overwrite the predicted time values with the observed values, essentially updating the timing of the predictions. By updating the timestamps on the predicted curve, operators can align the data to be processed more accurately.

### **7.3.2 Initial Nominal State Selection**

Once the curves are properly aligned in time, the nominal state vector is chosen at the discretion of the operator. The prediction file contains state vectors at each second. By rewriting the time stamps of the file, one is able to select any state vector that lies before all relevant observations.

In some instances it may be of value to choose the starting prediction value.

This would yield an updated version of the entire pass trajectory which may be of use in post-processing. Otherwise the initial nominal can be placed at the start of the observations. This choice is at the discretion of the user, and could be easily automated once the decision is made.

### 7.3.3 Orbit Prediction Results

The completion of mode two processing yields results that have the same defining characteristics of the results seen from mode one. These first visualizations provide comfort in knowing that the estimation process has at least preserved the main qualities of the orbit.

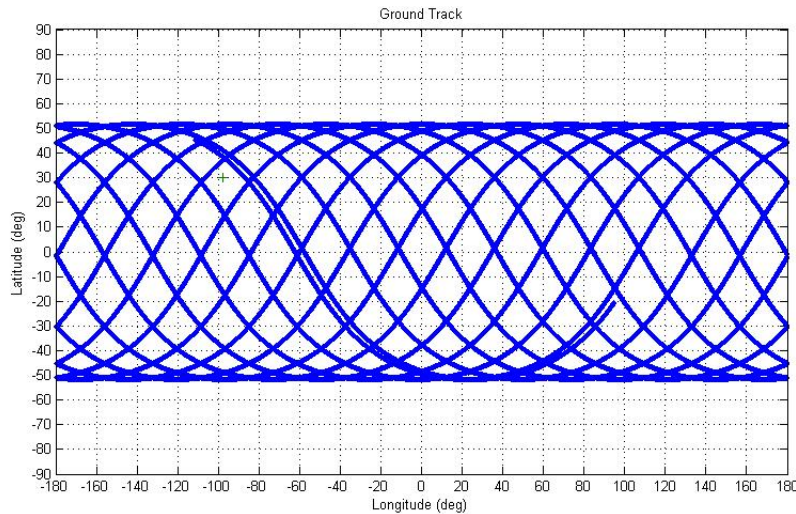


Figure 7.8: Ground track of the resulting 24-hour propagation from the starting time of pass used in mode two displays the two-dimensional trajectory of the spacecraft overlaying the Earth. This track overlaps the original from mode one for the time following the observed pass, but also continues forward until the new 24-hour propagation is complete.

The prediction results for mode two offer a display of what the next 24 hours



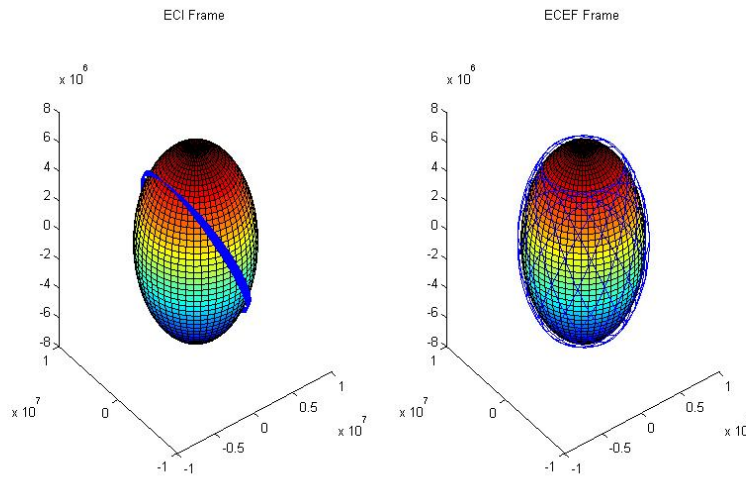


Figure 7.9: Three-dimensional plots of the spacecraft's trajectory seen in two different frames.

will look like for the satellite. It is important to note that there will be overlap in the results from mode one because the new propagation commences from the epoch used in the processing. For the new 24-hour period, there are predictions for seven satellite passes. The satellite passes are of relatively low elevations. This is due to the orbital geometry of the epoch which in this case has the satellite passing over the fringes of the visible area for the Texas Spacecraft Laboratory ground station.

Finally, one last comparison shows the selected pass elevation trajectory compared to the same pass after correction and processing. There are slight differences most notably in the peak elevations, but with respect to pointing an antenna with a beamwidth greater than a few degrees for simple communication and observation, the differences are tolerable.

Using the propagation technique in combination with the estimation process allows for a continuous cycle of predicting and correcting the orbit characteristics

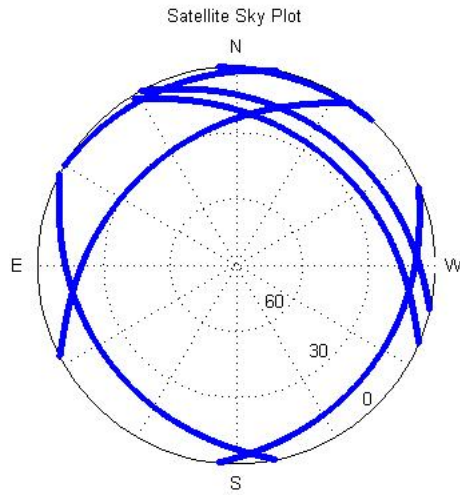


Figure 7.10: Skyplot displaying each of the seven overhead predicted passes.

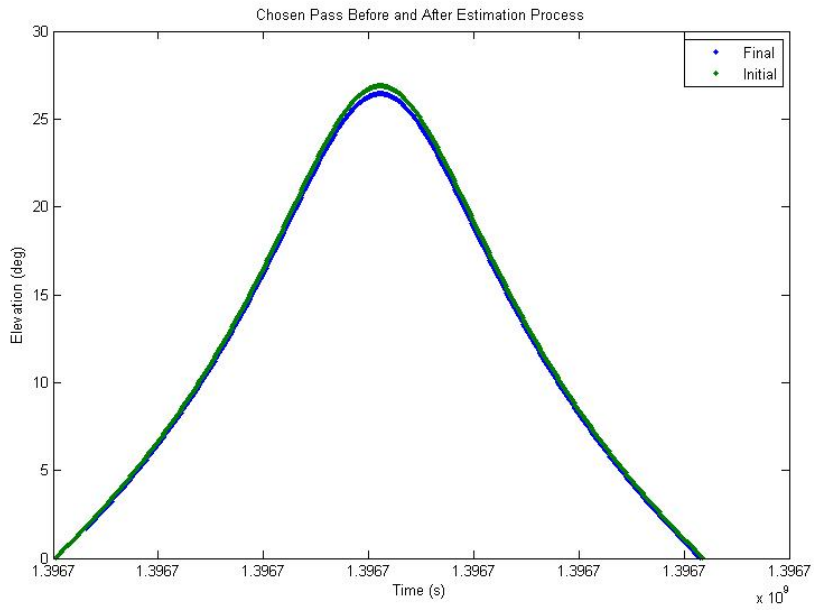


Figure 7.11: Elevation plots for the initial and the final trajectories for the processed pass.

for a specific satellite. By repeatedly undergoing the mode two procedures, manually or in an automated fashion, ground station operators can ensure that the satellite will not be lost.

As in the analysis for mode two, the speed of the code has not been discussed. The code was again written in Matlab for experimentation purposes. There is however the potential for real-time analysis. As stated earlier, this version uses a batch mode differential corrector requiring the full set of observations. Original code could be easily modified and adapted to run an extended sequential algorithm, yielding an updated value at each observation. This potential work has been left to future investigation. The most significant limitation of this tracking method is having only a single ground station to observe from. The processing could be greatly improved overall by the addition of ground stations spread over different areas in order to improve the overall geometry of the problem. By expanding the network of participating ground stations, operators could more accurately track cube satellites without significantly increasing costs.

## Chapter 8

### Conclusions and Future Work

#### 8.1 Conclusions

Cube satellite missions provide the aerospace community with a unique method of conducting numerous studies in the fields of both science and engineering. In order to adhere with the cube satellite standards, engineers must work to find methods of achieving complex mission goals while under tighter hardware constraints. This problem gives rise to the necessity for a ground-based tracking system that operators can use in order to continuously track the location of their satellite and the orbit characteristics. This thesis presents a method of using Doppler in coordination with reference TLE sets to satisfy those goals, and focuses on satellites that lack a GPS unit. Further, it discusses the opportunity for future expansion from one single station to a ground network run cooperatively to provide better tracking services for all cube satellite missions. This work is currently being implemented in ground station software to support upcoming missions of the Texas Spacecraft Laboratory.

As a single-station entity, the tracking program is able to establish a useable nominal orbit from the first mode of operation. After observing the satellite during a ground station pass, the measurements and subsequent Doppler calculations are fed into the second mode of operation where an estimation algorithm fits a new

trajectory. For high elevation passes, the geometry for the single ground station is better and thus provides more accurate results. For passes of lower elevations, the algorithm is strained and yields results with lesser confidence. Regardless, the fundamentals of the algorithm paired with the capable ground station provide a solid foundation for independently tracking cube satellite motion at a relatively low cost.

## **8.2 Future Work**

There are many possibilities for future work built upon this research. The first of which revolves around network expansion. Presently, the only ground station incorporating this type of software is the Texas Spacecraft Laboratory at the University of Texas, but by partnering with similar research groups at other universities or with amateur radio groups interested in supporting CubeSat missions, more can be done. By increasing the number of ground stations over a wide area, the number of strong satellite overhead passes would greatly increase, thus increasing the number of observations being recorded. This would lead to smaller error margins in the determined position and velocity of the satellite. The other main advantage of this cooperative network would be increased data recording time. The tight requirements for CubeSats limits the amount of data that can be sent back to Earth, but the one limiting factor has always been the low number of useable ground station passes. By increasing the number of spread out stations, more ground passes will allow for more data downlinks yielding more valuable science data.

Another area for more research to build upon what has been done here would

be to develop the software for a tracking network where multiple stations can send recorded observations, as well as query for information to use when updating orbit predictions and using differential correctors. The main focus for this area would be in networking and task automation.

A final area of investigation would be to continue looking at cheap tracking methods to use on cube satellites and other small budget missions. The subject of this research was primarily based on using Doppler updating and supplementary third party information in the form of TLEs. This information was used to guide a single communication antenna and schedule passes. For other research, this could be expanded using an array of ground antennas to further narrow down the ground-based direction of the signal, and back-tracking the information to be factored into the observation data.

## Bibliography

- [1] "An Analysis of State Vector Propagation using Differing Flight Dynamics Programs," AAS/AIAA Space Flight Mechanics Conference, Copper Mountain, Colorado 23-27 Jan. 2005. AAS Paper 05-199.
- [2] Bate, Roger R., Donald D. Mueller, and Jerry E. White. Fundamentals of Astrodynamics. New York: Dover Publications, 1971. 58-60.
- [3] Cable Installation Manual for Power and Control Cables. 9th ed. Highland Heights, Kentucky: General Cable Technologies Corporation, 2011. 17-18, 23-25, 76-79.
- [4] Davis, Philip J., and Philip Rabinowitz. Methods of Numerical Integration. New York: Academic Press, 1975. 271-274, 336-343.
- [5] "The Doppler Effect." The Doppler Effect. Accessed June 12, 2014.  
<http://m.teachastronomy.com/astropedia/article/The-Doppler-Effect>.
- [6] Dorrier, Jason. "Tiny CubeSat Satellites Spur Revolution In Space." Singularity HUB. June 23, 2013. Accessed October 5, 2014.  
<http://singularityhub.com/2013/06/23/tiny-cubesat-satellites-spur-revolution-in-space/>.
- [7] Dunbar, Brian. "Bigelow Spacecraft Carries NASA 'GeneBox' to Orbit." NASA. July 19, 2006. Accessed November 16, 2014.

- [http://www.nasa.gov/centers/ames/multimedia/images/2006/genebox\\_prt.htm](http://www.nasa.gov/centers/ames/multimedia/images/2006/genebox_prt.htm).
- [8] "Earthnet Online Geometry Glossary." European Space Agency. Accessed February 6, 2015. <https://earth.esa.int/handbooks/asar/CNTR5-5.html>.
- [9] Guier, William, and George Weiffenback. "Genesis of Satellite Navigation." Johns Hopkins Technical Digest 19, no. 1 (1998): 14-16.
- [10] Hsiao, Fei-Bin, Hui-Ping Liu, and Chung-Cheng Chen. "The Development of a Low-Cost Amateur Microsatellite Ground Station for Space Engineering Education." Global Journal of Engineering Education 4, no. 1 (200): 83-87.
- [11] Janssen, Nico. "Satellite TLE Object ID's." AMSATUK. March 8, 2014. Accessed May 24, 2014. <http://amsat-uk.org/2014/03/08/satellite-object-ids/>.
- [12] Kaula, William M. Theory of Satellite Geodesy; Applications of Satellites to Geodesy. Waltham, Mass.: Blaisdell Pub., 1966. 32-40, 56-57.
- [13] Kemble, Kyle. "Gibbs Method Orbit Determination." Cooperative Ground Station Orbit Determination. December 13, 2012. Accessed May 9, 2014. <https://sites.google.com/site/asen5050kemble/home>.
- [14] Larson, Wiley, and James Wertz. Space Mission Analysis and Design. 3rd ed. El Segundo, California: Microcosm Press, 1999. 624-628.
- [15] Malik, Tariq. "Antares Rocket Explosion: Full Coverage and Investigation | Space.com." Accessed October 31, 2015. <http://www.space.com/27594-private-antares-rocket-explosion-full-coverage.html>.



- [16] McHele, John. "NASA Uses Spectrum Software Defined Radio Technology for Satellite Communications." *Military & Aerospace Electronics*, May 1, 2003.
- [17] Mehrparvar, A., *CubeSat Design Specification*, Revision 13, The CubeSat Program, Cal Poly SLO, February 2014.
- [18] "Moon Motion." Moon Motion. Accessed July 15, 2014.  
<http://www.jgiesen.de/moonmotion/>.
- [19] "Nanosats Are Go!" *The Economist*. June 7, 2014. Accessed December 3, 2014. <http://www.economist.com/news/technology-quarterly/21603240-small-satellites-taking-advantage-smartphones-and-other-consumer-technologies>.
- [20] NASA CubeSats Initiative. Accessed October 18, 2014.  
[http://www.nasa.gov/directorates/heo/home/CubeSats\\_initiative.html](http://www.nasa.gov/directorates/heo/home/CubeSats_initiative.html).
- [21] "NORAD Two-Line Element Sets Current Data." CelesTrak: Current NORAD Two-Line Element Sets. Accessed January 13, 2014.  
<http://www.celestrak.com/NORAD/elements/>.
- [22] Rawashdeh, Samir A., and James E. Lumpp, Jr. "Aerodynamic Stability for CubeSats at ISS Orbit." *Journal of Small Satellites* 2, no. 1 (2013): 85-88.
- [23] Russell, Gregory. "Ink Markup Language." Ink Markup Language. Accessed November 6, 2014. <http://www.w3.org/TR/2003/WD-InkML-20030806/>.

- [24] Sakamoto, Yuji, Yoshitaka Kasahara, and Tetsuo Yasaka. "Low-Cost Orbit Determination System For A Cubesat." International CubeSat Symposium, 2003, 5-7.
- [25] "The Science Behind DANDE." Colorado Spacegrant DANDE. Accessed February 15, 2015. <http://spacegrant.colorado.edu/about-dande/science>.
- [26] Shampine, L. F., I. Gladwell, and S. Thompson. Solving ODEs with MATLAB. Cambridge: Cambridge University Press, 2003. 27-33.
- [27] "Smallsat Deployment." NanoRacks. Accessed September 28, 2014. <http://nanoracks.com/products/smallsat-deployment/>.
- [28] "Space, Stars, Mars, Earth, Planets and More - NASA Jet Propulsion Laboratory." Space, Stars, Mars, Earth, Planets and More - NASA Jet Propulsion Laboratory. Accessed February 10, 2013. <http://phaeton.jpl.nasa.gov/external/projects/race.cfm>.
- [29] Tapley, Byron D., and Bob E. Schutz. Statistical Orbit Determination. Amsterdam: Elsevier Academic Press, 2004. 82.
- [30] T. S. Kelso, "Validation of SGP4 and IS-GPS-200D Against GPS Precision Ephemerides," AAS/AIAA Space Flight Mechanics Conference, Sedona, Arizona. 28-31 Jan. 2007. AAS Paper 07-127.
- [31] Tobler De Sousa, Cristina, Helio Koiti Kuga, and Rodolpho Vilhena De Moraes. "Improving the Passive Doppler Geolocation System Through Extension of the Data Reception Network." Brazilian Journal of Geophysics 26, no. 4 (2008).

- [32] Vallado, D.A., Finkleman, D., 2008. A critical assessment of satellite drag and atmospheric density modeling, Paper AIAA 2008-6642, AIAA/AAS Astrodynamics Specialist Conference and Exhibit, Honolulu, Hawaii, USA, 18-21 August 2008.
- [33] Werner, Debra. "Small Satellite Launch Opportunities on the Rise - SpaceNews.com." SpaceNews.com. August 13, 2012. Accessed November 6, 2014. <http://spacenews.com/small-satellite-launch-opportunities-rise/>.